

Multi-fold increase in rainforests tipping risk beyond 1.5-2°C warming

Chandrakant Singh^{1,2,*}, Ruud van der Ent³, Ingo Fetzer^{1,2}, Lan Wang-Erlandsson^{1,2}

¹Stockholm Resilience Centre, Stockholm University, Stockholm, Sweden

²Bolin Centre for Climate Research, Stockholm University, Stockholm, Sweden

³Department of Water Management, Faculty of Civil Engineering and Geosciences, Delft University of Technology, Delft, The Netherlands

*Corresponding author; E-mail: chandrakant.singh@su.se

ORCID

Chandrakant Singh: <http://orcid.org/0000-0001-9092-1855>

Ruud van der Ent: <https://orcid.org/0000-0001-5450-4333>

Ingo Fetzer: <http://orcid.org/0000-0001-7335-5679>

Lan Wang-Erlandsson: <http://orcid.org/0000-0002-7739-5069>

Abstract. Tropical rainforests invest in their root systems to store soil moisture from water-rich periods for use in water-scarce periods. An inadequate root-zone soil moisture storage predisposes or forces these forest ecosystems to transition to a savanna-like state, devoid of their native structure and functions. Yet changes in soil moisture storage and its influence on the rainforest ecosystems under future climate change remain uncertain. Using the empirical understanding of root zone storage capacity, we assess the future state of the rainforests and the forest-savanna transition risk in South America and Africa under four different shared socioeconomic pathway scenarios. We find that by the end of the 21st century, nearly one-third of the total forest area will be influenced by climate change. Furthermore, beyond 1.5-2°C warming, ecosystem recovery reduces gradually, whereas the forest-savanna transition risk increases several folds. For Amazon, this risk can grow by about 1.5-6 times compared to its immediate lower warming scenario, whereas for Congo, this risk growth is not substantial (0.7-1.65 times). The insight from this study underscores the urgent need to limit global surface temperatures below the Paris agreement.

Introduction

Tropical rainforests in the Amazon and Congo basins are critical to the Earth system since they store and sequester a large amount of carbon, host vast biodiversity, and regulate the global water cycle¹. However, these forests are under severe pressure from climate change and land-use change²⁻⁴, with the risk of amplifying further warming and forest loss⁵. Climate change and land-use change lead to a decrease in precipitation, an increase in seasonality and atmospheric water demand¹. All of which create a deficit in soil moisture availability and inhibit plant growth^{6,7}. Furthermore, climate-induced hydroclimatic changes, including projected increases in drought frequency, severity, and duration^{8,9}, present threats to the capacity of rainforests to maintain their native ecological structure and functions (i.e., resilience)^{6,10-12}.

Under water-deficit, rainforests adapt by investing in their root systems to increase their capacity to access soil moisture^{6,13}. At the same time, the availability of surplus moisture at shallow depths minimises the need for ecosystems to invest in extensive (deeper and lateral) root systems¹⁴. Since the rooting structure is challenging to measure at the ecosystem scale¹⁵, previous studies have found that empirically-derived root zone storage capacity (S_r) correlates well with ecosystems' subsoil water storage and forest transition dynamics^{6,16,17}. Here, S_r constitutes a hydrological buffer required by the ecosystem for the collection of surplus precipitation from wet periods to be stored and used for evaporation throughout the dry periods (when total evaporation is greater than precipitation)^{6,16,18}. Therefore, a lowly water-stressed (defined based on the magnitude of deficit in soil moisture availability inhibiting plant growth) ecosystem will need the least investment to access stored moisture.

In contrast, a highly water-stressed ecosystem will require extensive subsoil investment⁶. However, S_r investment is costly, and there exists a ceiling up to where ecosystems cannot maximise their S_r any further⁶. Approaching this ceiling also implies that forest ecosystems are depleting their adaptive capacity towards further future hydroclimatic changes^{15,19,20}, with forests that have extended their S_r close to maximum being most vulnerable to increases in water-stress¹³. Excessive short-term water deficits in these forests lead to tree mortality, loss of carbon sink strength, and an increase in the risk of fire^{12,21,22}, whereas long-term water deficits can lead to large-scale tipping to a savannah-like state^{6,23,24}.

However, such ecohydrological dynamics remain challenging to incorporate in the Earth System Models (ESMs)²⁵⁻²⁷ – complex mathematical representations of Earth system processes and interactions across different biospheres. In contrast to empirical studies, the inherent lack of ecosystem-state variables²⁸, limited vegetation-climate feedbacks²⁹⁻³¹, subsoil moisture availability³² and adaptation dynamics³³, prescribed land-use change³⁴, and slow response time of forest ecosystems to climate change in the ESMs makes predicting (abrupt) forest-savanna transitions challenging^{35,36}. In addition, the risk of forest-savanna transitions under various possible climate future scenarios is relatively under-investigated. As a result of the conflicting findings and scenario-dependent uncertainties, the Intergovernmental Panel on Climate Change (IPCC) has only low

confidence about the possible tipping of the Amazon forest by the end of the 21st century³⁷. However, with mounting empirical evidence on how climate change influences rainforest ecosystems^{6,13,38,39}, the research on rainforest resilience loss has accelerated considerably in the recent decade^{40,41}. Yet, forest resilience is often assessed based on changes in forest carbon stocks^{41,42} or precipitation^{23,43,44}; and rarely on actual moisture storage capacity in the root zone¹³. Further, there is a need to assess and contrast the forest resilience consequences of low-emission and current commitment trajectories with the more commonly used high-emission scenario⁴⁵.

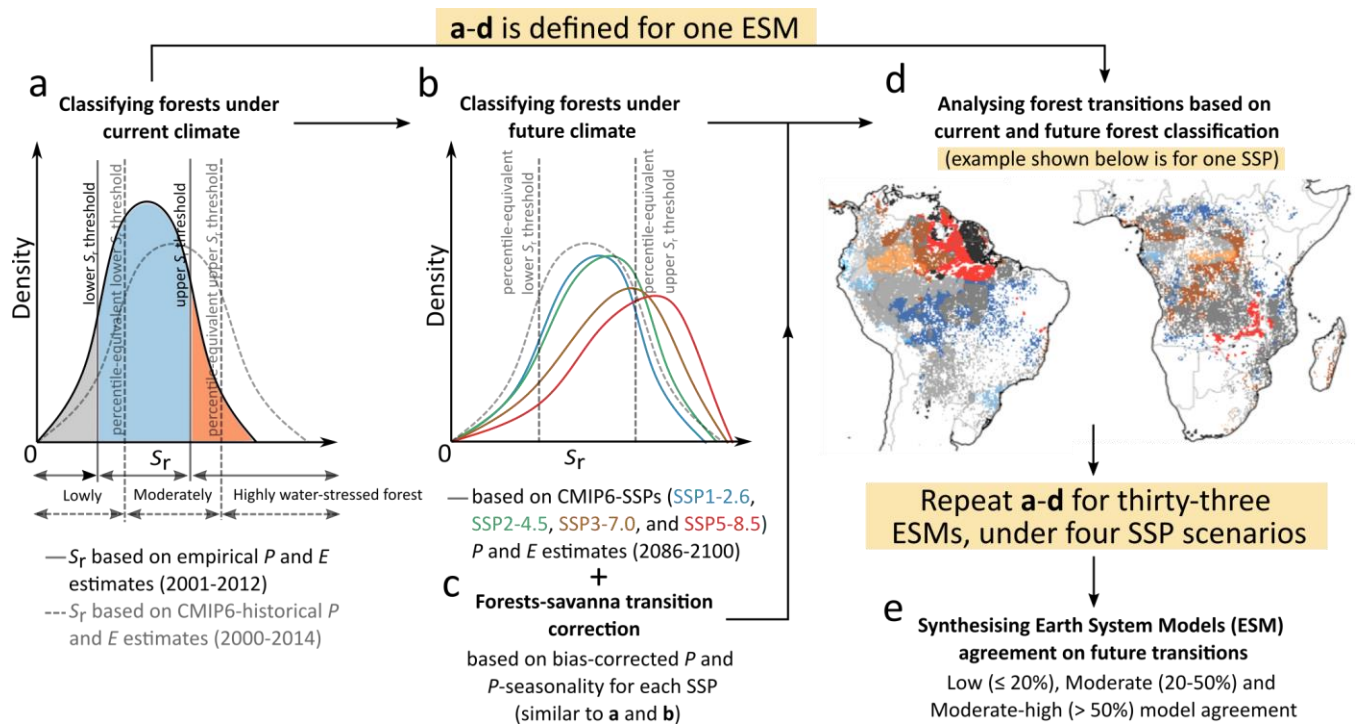


Figure 1 | Methodological framework for analysing the tropical forests transitions using empirical and CMIP6-Earth System Models (ESMs) estimates. (a) We use root zone storage capacity (S_r)-based forest classification, i.e., lowly, moderately, and highly water-stressed forests – calculated using empirical precipitation (P) and evaporation (E) estimates (Supplementary Figure 1; see methods). To compare the empirically derived S_r with individual CMIP6-ESMs derived S_r under the current climate, we bias-corrected the S_r thresholds for all ESMs using the histogram equivalence method (Supplementary Table 1). (b) We use these bias-corrected (percentile) S_r thresholds to classify the forests' state under future climate conditions (Supplementary Figures 2-3), (c) including correction for forest-savanna transitions (Supplementary Figure 4). (d) We then analyse the transitions between different forest states under current and future climate individually for all ESMs (see Supplementary Data). (e) Ultimately, we synthesise the results from all CMIP6-ESMs and discuss the agreement for the projected future state of the tropical forests by the end of the 21st century (Supplementary Figures 5-6). A detailed description is provided in the 'Methods' section. An exemplification of this methodological framework is shown in Supplementary Figure 7.

This study aims to assess the rainforest resilience and risk of a forest-savanna transition by the end of the 21st century based on an empirical understanding of ecosystems' subsoil dynamics. For this, we use hydroclimate-derived root zone storage capacity (S_r) (see methods), representing the maximum amount of soil

moisture that vegetation can access for transpiration^{6,16,46}. Compared to other statistical metrics^{39,47–49}, S_r provides an early indication of forest-savanna transition and a more comprehensive understanding of ecosystem dynamics under water-limiting conditions^{6,13}. Due to the considerable variability between hydroclimatic estimates from different ESMs, we assess resilience qualitatively by classifying forests. For this, we use S_r -based classification to categorise forests as lowly, moderately and highly-water stressed respectively (see methods). To make this classification comparable between empirical and Coupled Model Intercomparison Project Phase 6 (CMIP6) estimates from the ESMs, we first bias correct each (individual) ESM-derived S_r (2000–2014) with empirically derived S_r (2001–2012) under current climate using histogram equivalence method⁵⁰ (Figure 1a). These bias-corrected classification thresholds are then overlaid with future climate S_r for the same ESM to classify forests under future climate (2086–2100) (Figure 1b). Furthermore, we also correct for forest-savanna transition using bias-corrected precipitation and precipitation seasonality (Figure 1c). Based on this current and future classification, we evaluate potential transitions in the forest ecosystems for each ESM (Figure 1d). These steps are repeated for 33 ESMs (from 22 different institutes) under four different SSP scenarios (SSP1-2.6 leads to approx. 1.3–2.4°C warming; SSP2-4.5 corresponds to 2.1–3.5°C warming and is closest to the current trajectory according to the nationally determined contributions⁵¹; SSP3-7.0 around 2.8–4.6°C warming; and SSP5-8.5 represents 3.3–5.7°C warming; °C warming represents increase in mean global surface temperature change by the end of 21st century relative to 1850–1900⁵²), and ultimately synthesised for discussion (Figure 1e).

Results

In this study, we focus on three specific transitions: (i) Forest-savanna transition, (ii) forests' transition to a more water-stressed state, and (iii) reversion to a less water-stressed state (Figure 2a). We find that under future climate conditions (2086–2100), considering >50% models' agreement, about one-fourth of the forests in both South America and Africa are projected to transition (Figure 2b–g). With >20% models' agreement, these transitions are projected to occur for about three-fourths of the forests for both continents. Considering a lower threshold for models' agreement causes double or triple counting of some transitions (Figure 2b–g). To minimise this in further analyses, we only consider >50% models' agreement for forests that transition to a more and less water-stressed state. Furthermore, because (abrupt) forest-savanna transitions are under-represented in ESMs^{25–28}, we consider >20% models' agreement for them. Considering this, we not only reduce the overlap to <0.4% of total forest area (Supplementary Figure 8), but we also maximise highlighting forest-savanna transition risk for both continents.

We find that forest-savanna transitions mainly occur in the Guiana Shield of South America, and the southern and south-eastern regions of Africa (Figure 3). Compared to Africa, forest-savanna transitions are more prominent in South America under warmer climates (i.e., higher SSPs; Figures 2b and 3). Our analysis

reveals that the extent of forest-savanna transitions in South America decreases from almost $1.32 \times 10^6 \text{ km}^2$ (16.3% of total forest area in South America) under the highest emission scenario to $0.04 \times 10^6 \text{ km}^2$ (0.5%) under the lowest emission scenario (Figure 2b). Interestingly, for Africa, the extent of forest-savanna transition did not change much for different SSPs, i.e., (median) $0.25 \times 10^6 \text{ km}^2$ with a maximum deviation of $\pm 0.11 \times 10^6 \text{ km}^2$ (minimum and maximum extent of transition between 3-6.6% of total forest area in Africa) (Figure 2c). By evaluating changes to their hydroclimate, we find that under warmer climates, forest-savanna transition regions in both continents are projected to experience a decrease in precipitation. Furthermore, we observe an increase in precipitation seasonality for South America, whereas Africa shows a decrease (Supplementary Figure 11). Here, an increase in precipitation seasonality (seasonal variability in precipitation over the year) corresponds to water-deficit induced stress, whereas a decrease in seasonality and precipitation in Africa corresponds to a lower moisture availability altogether. Nevertheless, for both these continents, this transition seems to occur for the previously highly water-stressed forests under the current climate, followed by moderately, with the least contribution from lowly water-stressed forests (Figure 3). This highlights the looming risk on highly water-stressed forests to experience a forest-savanna transition under warmer climates.

Forests that transition to a 'more' water-stressed state, for South America are spatially aggregated towards the border between Brazil, Colombia, and Peru – covering a considerable portion of the Central Amazon (Figure 3). Whereas for Africa, these forests exist in moderate to small patches towards the northern and southern extent of central Congo rainforests. We observe that these transitions account for most of the projected changes to forests' states across both continents (Figure 2d,e), with the transition to just the 'highly water-stressed forest' accounting for more than three-fourths of all such transitions (Figure 3). We observe that South American forests gradually become increasingly water-stressed under warmer climates, with maximum and minimum projected transition of $1.89 \times 10^6 \text{ km}^2$ (23.4%) and $1.61 \times 10^6 \text{ km}^2$ (19.9%) observed under highest and lowest emission scenarios, respectively (Figure 2d,e). Whereas for Africa, the change in the water-stressed state of the forests under different SSP scenarios remain almost similar (i.e., median $1.14 (\pm 0.06) \times 10^6 \text{ km}^2$; 19.6-22.2%). Analysis of their hydroclimatic changes reveals that water-stress is induced by both a decrease in precipitation and an increase in seasonality in South America (Supplementary Figure 12). In contrast, water-stress in Africa is driven solely by an increase in seasonality. We observe that these newly water-stressed forests seem to have permeated to regions that were previously (under the current climate) dominated by lowly and moderately water-stressed forests (Figure 3). Here, this shift only signifies the changes to hydroclimatic conditions allowing forests to transition to a more water-stressed state, rather than the changes to the floristic composition of terrestrial species from one location to another. Although such a shift under changing climate is not unlikely⁵³, they are not analysed in this study.

Forests that revert to a 'less' water-stressed state, for South America are primarily observed in the south-eastern Amazon, with small patches observed towards eastern Brazil and the western coast of Equatorial

Guinea and Gabon (Figure 3). For Africa, the reverted forests exist in patches in the northern and southern regions of the Congo rainforest. Furthermore, for South America, we observe a gradual decrease in these reversions with an increase in warming. Here, we observe the lowest reversion of $0.23 \times 10^6 \text{ km}^2$ (2.8%) under the highest emission scenario and the highest reversion of $0.67 \times 10^6 \text{ km}^2$ (8.4%) under the lowest emission scenario (Figure 2f,g). For Africa, these trends remain almost similar under all SSPs (i.e., median $0.18 (\pm 0.05) \times 10^6 \text{ km}^2$; 2.2-3.5%). Comparing these transitions with their hydroclimatic changes reveals an overall increase in precipitation (Supplementary Figure 13). Interestingly, we observe a much higher precipitation increase for South America under high emission scenarios than those in lower emission scenarios. However, we find that precipitation seasonality is also higher for these ecosystems under warmer climates. This suggests that increased precipitation without changes to precipitation seasonality help decrease the water-stress of the ecosystem, compared to the ecosystems that experienced a simultaneous increase in both.

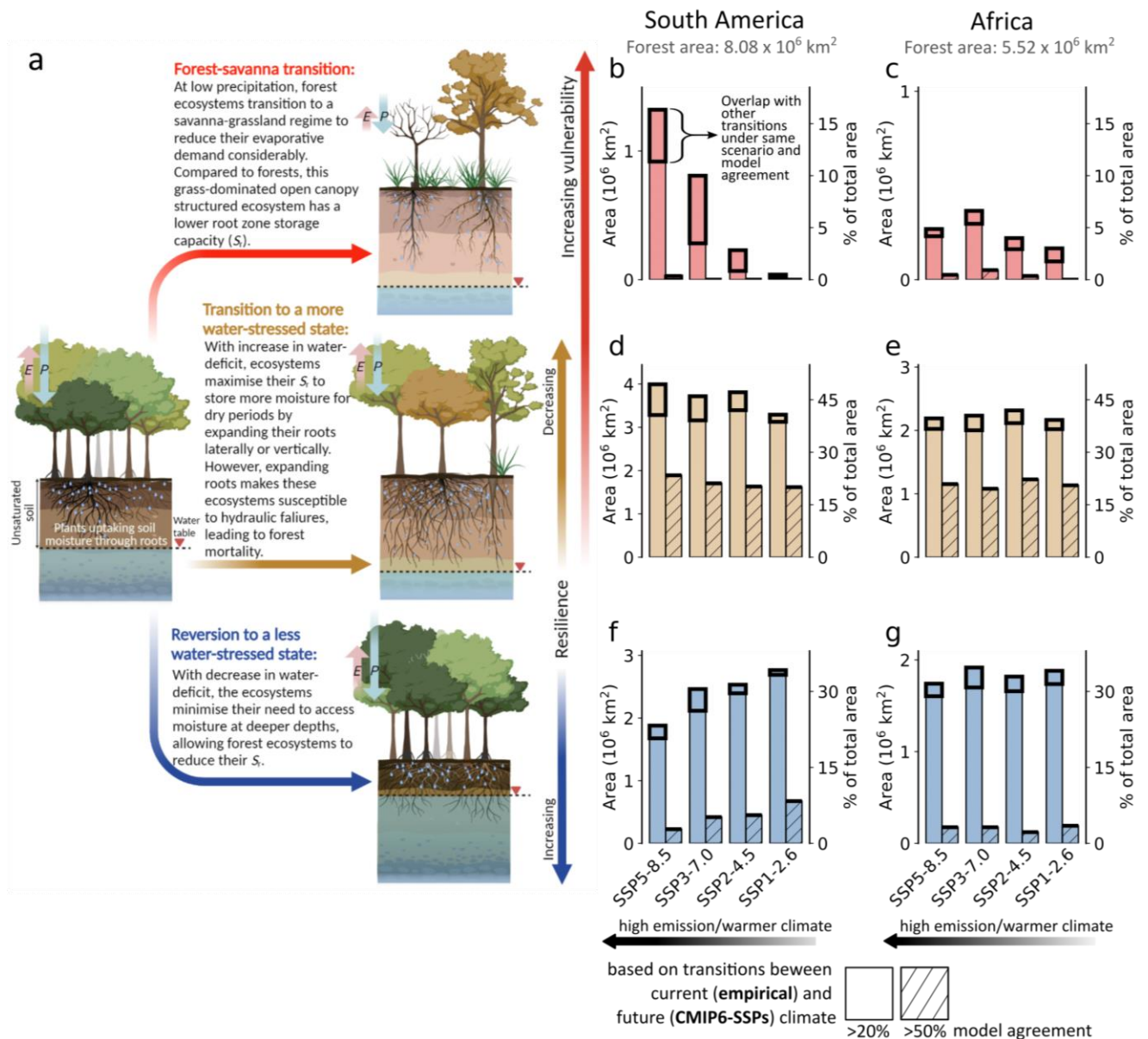
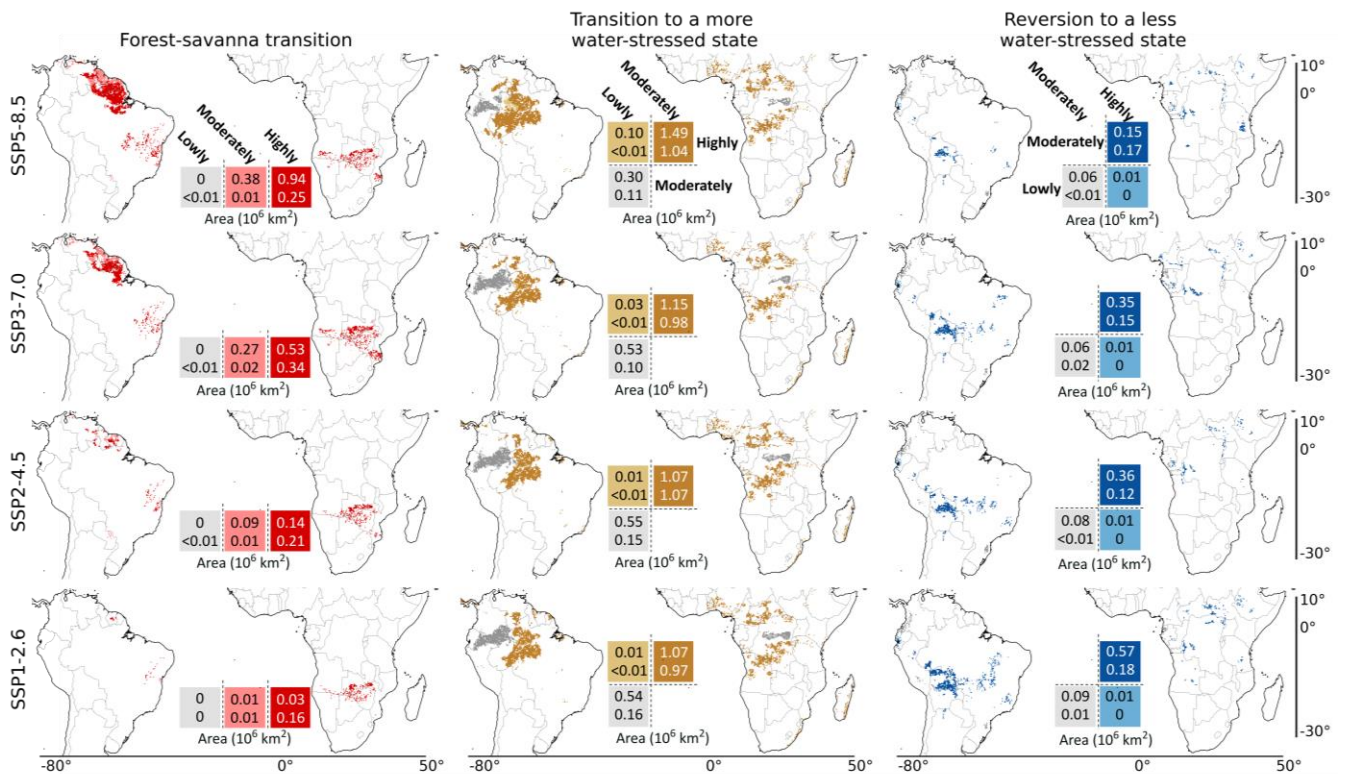


Figure 2 | Comparing the forest transitions under different SSP scenarios. (a) The state of the forest, both above- and below-ground, (post-transition) under future climate, quantifying (b,c) forest-savanna transition, (d,e) forests' that transition to a more water-stressed state and (f,g) revert to a less water-stressed state for South America and Africa (total forest area mentioned on the top of (b,c)), respectively. For the analysis above, transitions are calculated for pixels with model agreement >20% (plain bar plot) and >50% (hatched bar plot). These quantifications show changes to the forests' state based on empirical-current (2001-2012) and future (2086-2100) climate conditions. Analyses comparing forests' states based on CMIP6-historical (2000-2014) and future (2086-2100) climate conditions are shown in Supplementary Figures 9-10. For each transition, the total area of spatial overlap with other transitions under the same SSP scenario and model agreement is highlighted with thick black bars. The *P* and *E* arrows in (a) describe the relative magnitude of precipitation and evaporation fluxes. The illustration in (a) is adapted from ref.⁶ and created with BioRender.com.



Total forest area for South America: $8.08 \times 10^6 \text{ km}^2$
and Africa: $5.52 \times 10^6 \text{ km}^2$

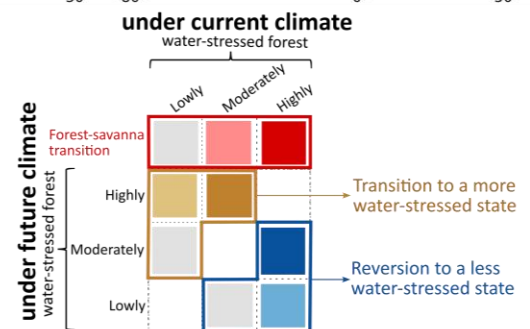


Figure 3 | Future rainforest transitions with respect to their current state under different SSP scenarios. We analysed forest transitions, explicitly focusing on forest-savanna transition, transition to a more water-stressed state, and reversion to a less water-stressed state, by comparing different forest classes under current (empirical; 2001-2012) and future (SSPs; 2086-2100) climate conditions (as defined in Figure 2). All transitions are analysed for moderate-high (>50%) model agreement, except forest-savanna transition, for which moderate

(>20%) model agreement is considered. Values overlaying the legends correspond to the total area of transition for South America (top values) and Africa (bottom values).

Discussion

Asynchronous resilience risks under future climate change. Our analysis reveals the spatial extent of future forest transitions in South America and Africa and their vulnerability to future climate change (Figures 2 and 4). For South America, we find a clear indication of a decrease in forest resilience (i.e., an increase in water-stressed forests) and an increase in forest-savanna transition risk under warmer climates (Figure 2b,d,f). In contrast, these trends are not symmetric for Africa, where transition risk shows only slight variation across the different SSPs (Figure 2c,e,g). Despite it being unclear to what extent the climate models represent the correct carbon dynamics³⁶, our results show a further divergence between Amazon's and Congo's responses to different SSPs (Figure 2 and Supplementary Figures 11-13). This could either be caused simply by a different response of precipitation patterns in the respective regions^{54,55} or to a different response to increased CO₂ levels in the atmosphere⁵⁶⁻⁵⁸.

Previous empirical studies have found that forest ecosystems in the Amazon are more dynamic – grow faster due to high CO₂ levels in the atmosphere – than those in the Congo rainforests. However, these fast-growing trees also die young due to them investing substantially less in their adaptive strategies against perturbations than (less dynamic) old-growth forests^{57,59}. This, combined with accelerated warming and frequent droughts faced by Amazon in recent decades, has made them more vulnerable to climate change than the Congo rainforests⁶⁰. For these ecosystems, the positive influence of CO₂ fertilisation-induced growth is counteracted by the negative impact of warming and droughts – thereby making the Amazon rainforest especially sensitive to CO₂ emissions pathways, which can exacerbate forest mortality under high emission scenarios^{56,57}. In this case, the projected changes to the future hydroclimate could be an artefact of forest mortality decreasing transpiration and precipitation over the rainforest. Previous studies also hint that these asynchronous resilience risks in the rainforest could be due to evolutionary biogeographical differences in the ecosystems leading to divergent species pools and resulting differences in ecosystems' functional attributes^{6,56,61}, and nutrient limitation⁶². According to them, the terrestrial species in Congo rainforests have already experienced severe droughts in the glacial periods, which makes them more adaptive to episodic water-induced perturbations than Amazon⁶³. Nevertheless, with compounding influence from land-use and climate-induced hydroclimatic changes⁴, these rainforests risk tipping to a savanna state. Our results highlight that by keeping the mean global surface temperature below 1.5-2°C warming (which in this case is equivalent to SSP1-2.6 relative to the pre-industrial), we minimise forest-savanna transition risk and maximise recovery – thereby improving the resilience of rainforest ecosystems (Figure 2).

Inferring adaptations from root zone storage capacity. We analyse S_r to relate changes in precipitation, precipitation seasonality and atmospheric water demand (Figures 1-2 and Supplementary Figures 11-13) with the ecosystem's dynamic subsoil adaptation⁶. Here, the observed transitions are the aftermath of the ecosystem's minimising and (as observed in most cases) maximising their subsoil storage capacity to offset water-deficit and efficiently utilise available subsoil moisture under future climate change (Figure 2a). Since plants prefer moisture uptake from the shortest pathway with least resistance, a decrease in water deficit – increase in precipitation, decrease in seasonality and atmospheric water demand – will enhance the availability of moisture at shallow depths and motivate vegetation to utilise shallow roots for moisture uptake¹⁴. This allows the forests to reduce their total subsoil storage capacity while transitioning towards a less water-stressed state^{6,14}.

However, an increase in water deficit forces forest ecosystems to invest in their subsoil structure and adapt strategies to store surplus moisture from wet seasons to ensure their survival during dry seasons, meaning that ecosystems transition to a more water-stressed state⁶. Furthermore, higher investment in deeper and extensive lateral roots exposes plants to embolism-related hydraulic failures⁶⁴, thus increasing forest mortality risk under droughts^{21,65,66}. This, along with other biotic and abiotic factors, including the maximum rooting extent of individual tree species^{67,68}, geological factors limiting roots to utilise deeper subsoil water and nutrient resources⁶⁹, and anaerobic conditions influencing microbial population at deeper depth⁷⁰, among others^{71,72}; caps the maximum adaptive capacity of the ecosystems to invest⁶ and may influence diverse adaptive behaviour between ecosystems⁷³. Under further episodic changes in soil moisture availability, i.e., beyond their maximum adaptive capacity, ecosystems survive by adapting to a new regime with relatively low moisture demand and more drought tolerance⁷⁴, which in this case is similar to a savanna ecosystem^{6,13}.

Changes in atmospheric moisture flows drive forest-savanna transitions. Among all transitions, the most noticeable and catastrophic (since it is difficult to revert) is the forest-savanna transition projected in the Amazon's Guiana Shield of South America, and over the southern and south-eastern part of Africa (Figures 2b,c and 3). These transitions are associated with the shifting of the inter-tropical convergence zone (ITCZ)⁷⁵, which decreases precipitation and increases precipitation seasonality over the continents. For South America, the creation of these low-pressure bands allows the trade winds to bring in considerable moisture from the equatorial Atlantic Ocean over to Amazon by passing through the Guiana Shield and ultimately carrying it across the La Plata Basin via the South American low-level jet⁷⁶⁻⁷⁸. Similarly, for Africa, where south-eastern trade winds bring moisture from the Indian Ocean over the centre of the African continent⁷⁵. Under a warmer climate, sea surface temperature over the equatorial Atlantic and the northern Indian Ocean is projected to increase^{79,80}, leading to a southward shift in ITCZ over the eastern Pacific and Atlantic Oceans, and northward over east Africa and the Indian Ocean^{75,81}. Previous studies also acknowledge that the intense surface warming over the Sahara

under future climate can also attract ITCZ northwards in Africa^{75,82,83}. Since these shifts in ITCZ can potentially both counteract and aggravate (especially critical for highly water-stressed forests) the impact of water-deficit, including those impacted by the localised deforestation⁸⁴⁻⁸⁷. It warrants the need to include changes in atmospheric circulation for studies analysing the impact of future climate on the resilience of natural and human-influenced systems^{43,44}.

Comparing prescribed future land-use with projected transitions. Besides different radiative forcing, the CMIP6-ESMs also use prescribed land-use scenarios for each SSP. Therefore, it is interesting to check whether these scenarios agree or conflict with the changes projected from our S_r -based classification method. Our analysis reveals that the extent of transitions is often underestimated in prescribed land-use than those analysed in this study (Figured 2-3 and Supplementary Figures 14-17), especially forest-savanna transitions (Supplementary Figure 14). This is because the prescribed land-use in CMIP6-ESMs is derived from Integrated Assessment Models (IAMs). However, unlike ESMs, which simulate physical Earth system processes, IAMs simulate macro-socioeconomic processes (e.g., spatial changes to croplands, irrigated areas, crop rotation, fertiliser rates on crops based on food demand) to determine land-use for future SSP scenarios^{34,88} – thereby not accounting for abrupt transitions in Earth systems⁸⁹, such as forest-savanna transition risks. Furthermore, since damages in IAMs are often represented by a smooth function of temperature^{89,90}, there is a potential for them to under- or overestimate naturally occurring land-use change⁹¹. These uncertainties in prescribed land-use can influence local land-use strategies (such as plantation) and undermine climate change mitigation efforts (e.g., the potential of restoration)⁹². In ESMs, this uncertainty can lead to variation in land cover dynamics and associated biophysical processes⁹³ (e.g., if the prescribed land use is defined as forest instead of rangeland, it will directly impact on water cycle due to erroneous estimates of evaporation, runoff and infiltration)^{40,94} – thereby leading to unrealistic perception of future forest transitions (Supplementary Figures 14-17). By analysing forest transitions based on hydroclimate-derived S_r , we highlighted the inconsistencies in prescribed land-use solely based on IAMs. Circumventing this requires a more dynamic and combined assessment of climate and socioeconomic factors and their impacts to assess land-use change, potential tipping risks in the terrestrial ecosystems and associated societal risks⁹⁵.

Sensitivity analyses. Forest transitions are sensitive to hydroclimatic changes and adaptive strategies of the ecosystems. We perform sensitivity analyses on S_r (representing S_r -based adaptation) and forest-savanna transition thresholds to check the robustness of the projected transitions (Figures 1-2 and Supplementary Figures 17-21). We observe that increase in lower and upper S_r thresholds leads to more ecosystems transitioning to a ‘more’ or ‘less’ water-stressed state (Supplementary Figures 18-19). Whereas a decrease in forest-savanna transition thresholds (i.e., precipitation and precipitation seasonality; relative to Figure 4) leads to a reduction in forest-savanna transition risk (Supplementary Figures 20-21). Furthermore, fixing an extreme

S_r threshold – signifying forest-savanna transition for ecosystems that cannot maintain their above-ground structure at high S_r – we observe some shifts close to the already projected risk regions and coastal regions (Figure 3 and Supplementary Figure 17). However, this transition risk in the coastal regions could be an artefact of interpolating hydroclimate estimates to higher resolution, and since oceans have a more prevalent evaporation than land – it could lead to high S_r and therefore projection of tipping risk in coastal regions. Nevertheless, for all these sensitivity analyses, the differences in the magnitude of transitions are minor; however, the trends between different SSP scenarios remain almost similar for both continents (Figure 2 and Supplementary Figures 18-21). This means that despite the changes in factors that can influence forest transition, the conclusions drawn from this study do not change.

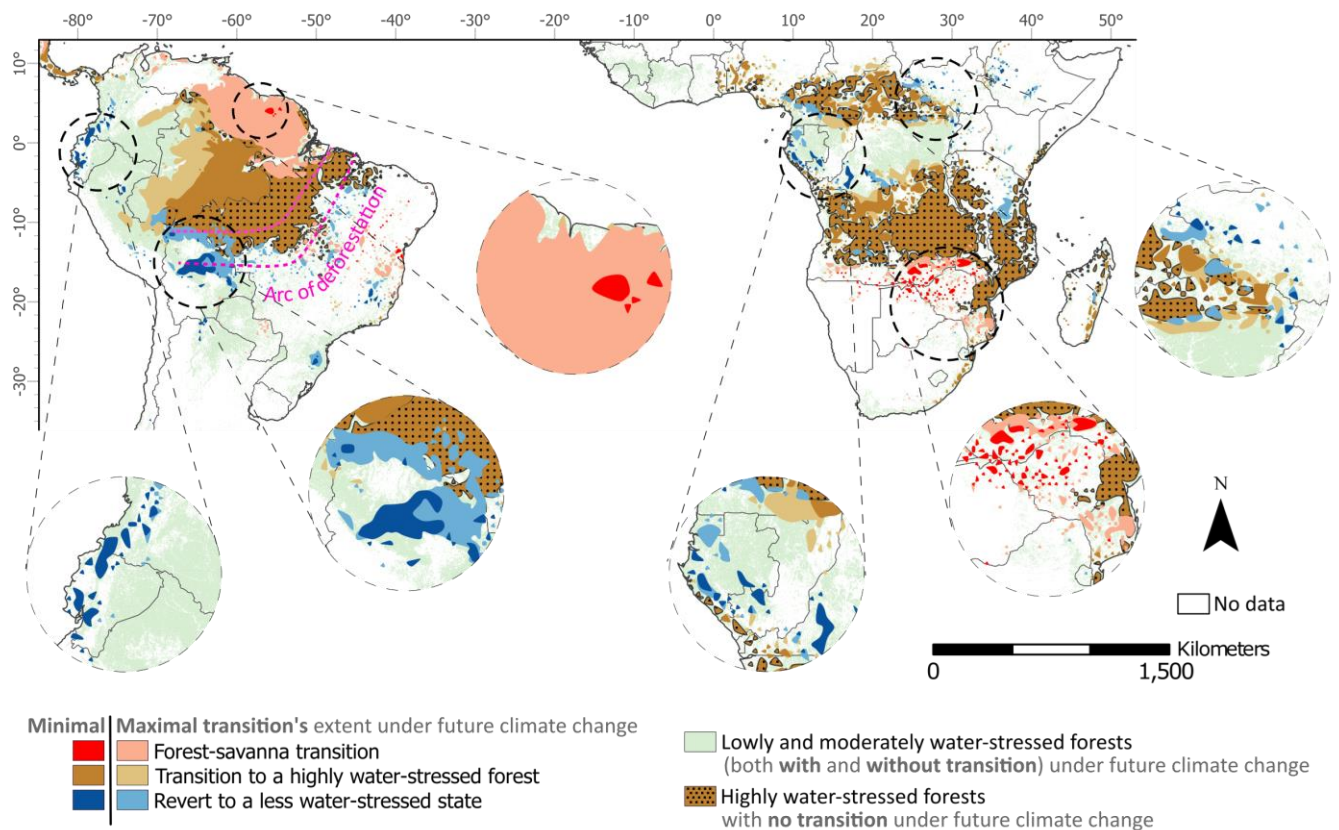


Figure 4 | Minimal and maximal extent of potential forest transitions under future climate change in the entire study region over South America and Africa. The three forest transition types are: from forest to savanna, from any class to highly water-stressed forests, and from any class to a less water-stress state (see definitions in Figures 2-3). The minimal and maximal represents the minimum and maximum possible extent of transitions (as quantified in Figure 3) based on changes between current (empirical; 2001-2012) and future (SSPs; 2086-2100) climate conditions regardless of the SSP scenarios.

In summary, classifying forest ecosystems based on empirical and CMIP6 ESMs-derived S_r – the ecosystem's capacity to store surplus moisture and access moisture during dry periods – allowed us to assess the future transitions in the rainforest ecosystems. The lowest emission scenario minimises rainforest tipping risks and maximises reversion to less water-stressed states, whereas the opposite is achieved in the high emission

scenario. In the Amazon rainforest, forest-to-savanna transition risks increase non-linearly with each degree of warming. In contrast, the risk increase between different emission scenarios is not significant for Congo. We believe that the results from this study can be used to further assess the direct and cascading influence of ecosystem transitions under future climate change on other natural and human-influenced systems (e.g., influence of rainforest tipping on downwind rainfall, agricultural production and global food supply chain). We find very limited tipping risk that is 'unavoidable', whereas the vast majority of potential transition risks can still be avoided by steering towards a less severe climate scenario, highlighting the window of opportunity. Furthermore, regions projected to transition to less water-stressed state can potentially become easier to restore and respond well to deforestation prevention measures. This study highlights the importance of restricting temperature change below 1.5-2°C warming relative to the pre-industrial global surface temperatures to prevent forest transition risks and provide the best conditions for effective ecosystem stewardship.

Methods

Study Area. This study focuses on forest ecosystems extending between 15°N–35°S for South America and Africa.

Data. This analysis uses both empirical and ESM-simulated datasets of precipitation and evaporation. Empirical datasets include remotely sensed and observation-corrected precipitation and evaporation time-series. Precipitation estimates at daily timestep are obtained from the Climate Hazards Group InfraRed Precipitation with Station data (CHIRPS; 0.25° resolution)⁹⁶. Furthermore, evaporation is derived using an equally-weighted ensemble of three different datasets – (i) Breathing Earth System Simulator (BESS; 0.5° resolution)⁹⁷ (ii) Penman-Monteith-Leuning (PML; 0.5° resolution)⁹⁸ and (iii) FLUXCOM-RS (0.083° resolution)⁹⁹ – at monthly timestep. Here, evaporation represents the sum of all evaporated moisture from soil, open water and vegetation, including interception and transpiration. We only selected evaporation datasets that are free from biome-dependent parameterisation (such as plant function types, stomatal conductance, maximum root allocation depth) and soil layer depth (represents maximum depth of moisture uptake). Ultimately, all evaporation datasets are bilinearly interpolated to 0.25° resolution and downscaled to daily timestep using ERA5 evaporation (0.25° resolution) estimates¹⁰⁰. All empirical datasets are obtained for 2001-2012.

From ESM-simulated datasets, we obtained precipitation and evaporation estimates for CMIP6-historical and -SSP simulations, i.e., SSP1-2.6, SSP2-4.5, SSP3-7.0 and SSP5-8.5 (33 ESMs from 22 different institutes; Supplementary Table 1-2). The historical estimates are obtained at a monthly timestep for 2000-2014 and the

estimates under different SSPs are obtained for 2086-2100. Though obtained moisture estimates from different ESMs are at different spatial resolutions, we bilinearly interpolated them to 0.25° for this analysis.

Lastly, we used land-cover data to we remove pixels with human influence and non-terrestrial landcover from our analysis to minimise influence on the natural water cycle. The landcover data used is the European Space Agency's (ESA's) global landcover classification – Globcover¹⁰¹ (originally 300m resolution, resolved to 0.25° resolution using majority interpolation).

Classifying forest under current and future climate conditions. We classify forests under current climate based on root zone storage capacity S_r , which represents the maximum amount of moisture accessed by vegetation for transpiration and is derived using mass-balance approach^{6,16}. First, S_r is derived using a mass-balance approach that determines maximum annual accumulated water deficit from daily estimates of precipitation and evaporation over several years (2001-2012 in this case) with a 20-year drought return period (Supplementary Method). This methodology assumes that ecosystems do not invest in expanding their storage more than necessary to bridge the water-deficit experienced by the vegetation in dry periods (i.e., periods in which evaporation is greater than rainfall, irrespective of the seasons). Furthermore, using empirical (observation-based) datasets, we capture the actual state of the ecosystems – reflecting the actual soil moisture availability for the ecosystems⁶.

Second, based on S_r ⁶, forest ecosystems in the tropics are classified into the three categories lowly, moderately and highly water-stressed forest. Since this study evaluates future forest transitions from several ESMs, all simulating Earth system state based on their unique parameterisations and biases – thereby creating variability between simulated estimates^{33,102,103}, we chose to assess forest's water-stressed state qualitatively by classifying forests. This classification is based on empirically observed trends in ecosystem's above- and below-ground structure, hydrology, and hydroclimate. Here, lowly, moderately and highly water-stressed forest correspond to state of the forest under different levels of water stress (i.e., quantifying magnitude and duration of water-deficit experienced by vegetation which can inhibit plant growth). Using the empirically defined S_r thresholds⁶ (Figure 1; Supplementary Table. 1), we classified forest under current climate.

For South America, these empirical S_r thresholds are ≤ 100 mm (for lowly; also referred to as 'lower S_r threshold'), 100-400 mm (for moderately) and >400 mm (for highly water-stressed forest; also referred to as 'upper S_r threshold') (Figure 1a). For Africa, these S_r thresholds are ≤ 100 mm (for lowly), 100-350 mm (for moderately) and >350 mm (for highly water-stressed forest). Higher S_r implies a need for larger storage to buffer water deficit, which previous studies found corresponds to plants expanding their roots both vertically and laterally to maximise storage. However, compared to the ecosystems root-relevant characteristics, which are difficult to measure at ecosystem scale, mass-balance approach-based S_r provides a tangible and comprehensive understanding of ecosystem subsoil dynamics.

As mentioned previously, different ESMs are based on different research groups' understandings of Earth system processes and are therefore parameterised differently^{102,103}. Therefore, it does not make sense to directly use the empirical (2001-2012) S_r thresholds to compare ecosystems' state for CMIP6-ESMs under current climate conditions. Furthermore, since daily estimates of precipitation and evaporation are not publicly available for all CMIP6-ESM simulations, it would not be logical to directly compare them with monthly precipitation and evaporation derived S_r (method for calculating S_r from CMIP6 estimates remains same; Supplementary Method and Supplementary Figure 22). To resolve this, we used the histogram equivalence method⁵⁰. Here, the percentile-equivalent for the empirical S_r thresholds is calculated individually for thirty-three CMIP6-ESMs under current climate (CMIP6-historical between 2000-2014). For example, if a S_r of 100 mm correspond to 10th percentile in the empirically-derived S_r sample ($n = 20\%$ of total pixels), the 10th percentile equivalent in CMIP6-historically-derived S_r is considered its equivalent, but this can be higher or lower than 100 mm (Figure 1 and Supplementary Table 1).

Percentile-equivalent S_r thresholds are calculated for all ESMs individually under current climate conditions (i.e., using CMIP6-historical estimates between 2000-2014) (Figure 1a). These histograms analysed thresholds are referred to as percentile-equivalent lower and upper S_r threshold. To classify forest under future climate (2086-2100), we directly overlay the CMIP6-historically (2000-2014) evaluated percentile equivalent lower and upper S_r threshold to CMIP6-SSP derived S_r (2086-2100) – representing water-stressed state of the forest in the future (Figure 1b).

Forest-savanna transition correction. When analysing the future state of the forests, there is a possibility that a forest ecosystem has already transitioned to a savanna or grassland ecosystem. Savanna and grassland ecosystems experience considerably less precipitation and can show high precipitation seasonality. However, they may have S_r similar to that of lowly water-stressed forests due to their low evaporation. To account for such transitions, we did an additional analysis to segregate forests from savanna-grassland ecosystems. We did this by using mean annual precipitation and the precipitation seasonality index for all forest classes (Supplementary Figure 4). Here, we separated ecosystems falling outside the extent mean annual precipitation and precipitation seasonality index and classified them as 'savanna-grassland regime'. Additionally, to check for forest transitions to a savanna-grassland regime that might not have been accounted in prescribed land-use, but are still likely to occur in reality because some ecosystems could not maintain their structure and functions with a high S_r , we did an extreme value analysis (Supplementary Figure 17). However, since rate of transition of forest ecosystems to savanna is highly debatable/uncertain^{63,104,105}, we refer to them as forest-savanna transition, signifying the likelihood to a forest-savanna transition due to changes in their hydroclimate (Supplementary Figure 4).

Analysing and synthesising forest transitions under future climate change. Based on forest classification under current and future climate, we analyse forest transition, specifically focussing on forest-savanna transitions, forest ecosystems that will become more water-stressed in the future, those that will revert to a less water-stressed state by the end of the 21st century (Figure 1d). We synthesise the results from all CMIP6-ESMs representing future state of the forests under different SSP scenarios and their transitions with respect to the current climate, including those derived from both empirical (2000-2014) and CMIP6-historical (2000-2014) estimates (Figure 1e). Here, pixels with > 50% of model convergence are classified as ‘moderate-high model agreement’, 20-50% as ‘moderate model agreement’ and ≤ 20% as ‘low model agreement’.

Sensitivity analyses. To check the robustness of our analysis, we did two sensitivity analysis: (i) by changing the lower and upper S_r threshold (Figure 1a, Supplementary Figures 18-19), and (ii) by changing the forest-savanna transition thresholds (Supplementary Figures 4, 17, 20 and 21). Results from these sensitivity analyses are presented in Supplementary Figures 17-21.

Data availability

All the datasets that support the findings of this study are publicly available at: (CMIP6; citations referred to in Supplementary Table 2) <https://aims2.llnl.gov/>, (Root zone storage capacity; empirical) <https://github.com/chandrakant6492/Drought-coping-strategy>, (P-CHIRPS) <https://data.chc.ucsb.edu/products/CHIRPS-2.0/>, (E-BESS) <ftp://147.46.64.183/>, (E-FLUXCOM) <ftp.bgc-jena.mpg.de>, (E-PML) <https://data.csiro.au/collections/#collection/Cicsiro:17375v2>, (E-ERA5) <https://cds.climate.copernicus.eu/cdsapp#!/dataset/reanalysis-era5-single-levels>, (Globcover) http://due.esrin.esa.int.ezp.sub.su.se/page_globcover.php. Forest transitions for each ESM based on comparison between empirical (2001-2012) and SSP (2086-2100) scenarios are presented in Supplementary Data. Furthermore, all the data generated during this study will be made publicly available at Zenodo before the final acceptance of this manuscript.

Code availability

The python-language scripts used for the analyses presented in this study are available from GitHub: <https://github.com/chandrakant6492/Future-forest-transitions-CMIP6>. The python-language code for calculating (empirical) root zone storage capacity is available from GitHub: <https://github.com/chandrakant6492/Drought-coping-strategy>.

Acknowledgements

C.S., I.F. and L.W.-E. acknowledge funding support from the European Research Council (ERC) project ‘Earth Resilience in the Anthropocene’, project number ERC-2016-ADG-743080. L.W.-E. also acknowledges funding support from the Swedish Research Council for Sustainable Development (FORMAS), project number 2019-01220. R.v.d.E. acknowledges funding support from the Netherlands Organisation for Scientific Research (NWO), project number 016.Veni.181.015. The authors also acknowledge the computational support provided by Microsoft Planetary Computer (<https://planetarycomputer.microsoft.com>) for performing the analyses.

Author contributions

All authors contributed to conceptualisation of this research. CS performed the analyses and wrote the initial draft. All authors contributed to the discussion and revision leading to the final version of the manuscript.

Competing interests

The authors declare no competing interests.

References

1. Malhi, Y., Gardner, T. A., Goldsmith, G. R., Silman, M. R. & Zelazowski, P. Tropical Forests in the Anthropocene. *Annu. Rev. Environ. Resour.* **39**, 125–159 (2014).
2. Malhi, Y. *et al.* Climate Change, Deforestation, and the Fate of the Amazon. *Science* **319**, 169–172 (2008).
3. Lewis, S. L., Edwards, D. P. & Galbraith, D. Increasing human dominance of tropical forests. *Science* **349**, 827–832 (2015).
4. Davidson, E. A. *et al.* The Amazon basin in transition. *Nature* **481**, 321–328 (2012).
5. Lawrence, D., Coe, M., Walker, W., Verchot, L. & Vandecar, K. The Unseen Effects of Deforestation: Biophysical Effects on Climate. *Frontiers in Forests and Global Change* **5**, (2022).
6. Singh, C., Wang-Erlandsson, L., Fetzer, I., Rockström, J. & Ent, R. van der. Rootzone storage capacity reveals drought coping strategies along rainforest-savanna transitions. *Environ. Res. Lett.* **15**, 124021 (2020).
7. Wang-Erlandsson, L. *et al.* A planetary boundary for green water. *Nat Rev Earth Environ* **3**, 380–392 (2022).
8. Dai, A. Drought under global warming: a review. *WIREs Climate Change* **2**, 45–65 (2011).
9. Liu, W. *et al.* Global drought and severe drought-affected populations in 1.5 and 2 °C warmer worlds. *Earth System Dynamics* **9**, 267–283 (2018).
10. Grimm, N. B. *et al.* The impacts of climate change on ecosystem structure and function. *Frontiers in Ecology and the Environment* **11**, 474–482 (2013).
11. Jones, C., Lowe, J., Liddicoat, S. & Betts, R. Committed terrestrial ecosystem changes due to climate change. *Nature Geosci* **2**, 484–487 (2009).
12. Bauman, D. *et al.* Tropical tree mortality has increased with rising atmospheric water stress. *Nature* 1–6 (2022) doi:10.1038/s41586-022-04737-7.
13. Singh, C., van der Ent, R., Wang-Erlandsson, L. & Fetzer, I. Hydroclimatic adaptation critical to the resilience of tropical forests. *Global Change Biology* **28**, 2930–2939 (2022).
14. Bruno, R. D., Rocha, H. R. da, Freitas, H. C. de, Goulden, M. L. & Miller, S. D. Soil moisture dynamics in an eastern Amazonian tropical forest. *Hydrological Processes* **20**, 2477–2489 (2006).
15. Fan, Y., Miguez-Macho, G., Jobbágy, E. G., Jackson, R. B. & Otero-Casal, C. Hydrologic regulation of plant rooting depth. *Proceedings of the National Academy of Sciences* **114**, 10572–10577 (2017).
16. Wang-Erlandsson, L. *et al.* Global root zone storage capacity from satellite-based evaporation. *Hydrology and Earth System Sciences* **20**, 1459–1481 (2016).
17. de Boer-Euser, T., McMillan, H. K., Hrachowitz, M., Winsemius, H. C. & Savenije, H. H. G. Influence of soil and climate on root zone storage capacity. *Water Resources Research* **52**, 2009–2024 (2016).
18. Grossiord, C. *et al.* Plant responses to rising vapor pressure deficit. *New Phytologist* **226**, 1550–1566 (2020).
19. Kleidon, Axel. & Heimann, M. A method of determining rooting depth from a terrestrial biosphere model and its impacts on the global water and carbon cycle. *Global Change Biology* **4**, 275–286 (1998).
20. Guswa, A. J. The influence of climate on root depth: A carbon cost-benefit analysis. *Water Resources Research* **44**, W02427 (2008).
21. Aleixo, I. *et al.* Amazonian rainforest tree mortality driven by climate and functional traits. *Nat. Clim. Chang.* **9**, 384–388 (2019).
22. van Nes, E. H. *et al.* Fire forbids fifty-fifty forest. *PLOS ONE* **13**, e0191027 (2018).

23. Hirota, M., Holmgren, M., Van Nes, E. H. & Scheffer, M. Global Resilience of Tropical Forest and Savanna to Critical Transitions. *Science* **334**, 232–235 (2011).
24. Staver, A. C., Archibald, S. & Levin, S. A. The Global Extent and Determinants of Savanna and Forest as Alternative Biome States. *Science* **334**, 230–232 (2011).
25. Lenton, T. M. Early warning of climate tipping points. *Nature Clim Change* **1**, 201–209 (2011).
26. Maslin, M. & Austin, P. Climate models at their limit? *Nature* **486**, 183–184 (2012).
27. Valdes, P. Built for stability. *Nature Geosci* **4**, 414–416 (2011).
28. Drijfhout, S. *et al.* Catalogue of abrupt shifts in Intergovernmental Panel on Climate Change climate models. *Proceedings of the National Academy of Sciences* **112**, E5777–E5786 (2015).
29. Chai, Y. *et al.* Constraining Amazonian land surface temperature sensitivity to precipitation and the probability of forest dieback. *npj Clim Atmos Sci* **4**, 1–7 (2021).
30. Boulton, C. A., Good, P. & Lenton, T. M. Early warning signals of simulated Amazon rainforest dieback. *Theor Ecol* **6**, 373–384 (2013).
31. Boulton, C. A., Booth, B. B. B. & Good, P. Exploring uncertainty of Amazon dieback in a perturbed parameter Earth system ensemble. *Global Change Biology* **23**, 5032–5044 (2017).
32. Cheng, S., Huang, J., Ji, F. & Lin, L. Uncertainties of soil moisture in historical simulations and future projections. *Journal of Geophysical Research: Atmospheres* **122**, 2239–2253 (2017).
33. Yuan, K., Zhu, Q., Riley, W. J., Li, F. & Wu, H. Understanding and reducing the uncertainties of land surface energy flux partitioning within CMIP6 land models. *Agricultural and Forest Meteorology* **319**, 108920 (2022).
34. Hurtt, G. C. *et al.* Harmonization of global land use change and management for the period 850–2100 (LUH2) for CMIP6. *Geoscientific Model Development* **13**, 5425–5464 (2020).
35. Hall, A., Cox, P., Huntingford, C. & Klein, S. Progressing emergent constraints on future climate change. *Nat. Clim. Chang.* **9**, 269–278 (2019).
36. Koch, A., Hubau, W. & Lewis, S. L. Earth System Models Are Not Capturing Present-Day Tropical Forest Carbon Dynamics. *Earth's Future* **9**, e2020EF001874 (2021).
37. Canadell, J. G. *et al.* Global Carbon and other Biogeochemical Cycles and Feedbacks. in *IPCC AR6 WGI, Final Government Distribution* chapter 5 (2021).
38. Küçük, Ç. *et al.* Characterizing the Response of Vegetation Cover to Water Limitation in Africa Using Geostationary Satellites. *Journal of Advances in Modeling Earth Systems* **14**, e2021MS002730 (2022).
39. Boulton, C. A., Lenton, T. M. & Boers, N. Pronounced loss of Amazon rainforest resilience since the early 2000s. *Nat. Clim. Chang.* **12**, 271–278 (2022).
40. Ahlström, A. *et al.* Hydrologic resilience and Amazon productivity. *Nature Communications* **8**, 387 (2017).
41. Huntingford, C. *et al.* Simulated resilience of tropical rainforests to CO₂-induced climate change. *Nature Geosci* **6**, 268–273 (2013).
42. Parry, I., Ritchie, P. & Cox, P. *Evidence of Amazon rainforest dieback in CMIP6 models.* <https://egusphere.copernicus.org/preprints/2022/egusphere-2022-82/> (2022) doi:10.5194/egusphere-2022-82.
43. Staal, A. *et al.* Hysteresis of tropical forests in the 21st century. *Nat Commun* **11**, 4978 (2020).
44. Zemp, D. C. *et al.* Self-amplified Amazon forest loss due to vegetation-atmosphere feedbacks. *Nature Communications* **8**, 14681 (2017).
45. Jehn, F. U. *et al.* Focus of the IPCC Assessment Reports Has Shifted to Lower Temperatures. *Earth's Future* **10**, e2022EF002876 (2022).
46. Gao, H. *et al.* Climate controls how ecosystems size the root zone storage capacity at catchment scale: Root zone storage capacity in catchments. *Geophysical Research Letters* **41**, 7916–7923 (2014).
47. Carpenter, S. R. & Brock, W. A. Rising variance: a leading indicator of ecological transition. *Ecology Letters* **9**, 311–318 (2006).
48. Rocha, J. C. Ecosystems are showing symptoms of resilience loss. *Environ. Res. Lett.* **17**, 065013 (2022).
49. Dakos, V. *et al.* Slowing down as an early warning signal for abrupt climate change. *Proceedings of the National Academy of Sciences* **105**, 14308–14312 (2008).

50. Piani, C. *et al.* Statistical bias correction of global simulated daily precipitation and temperature for the application of hydrological models. *Journal of Hydrology* **395**, 199–215 (2010).
51. *The Paris Agreement | UNFCCC*. https://unfccc.int/sites/default/files/english_paris_agreement.pdf (2015).
52. IPCC. Summary for Policymakers. *Climate Change 2021: The Physical Science Basis. Contribution of Working Group I to the Sixth Assessment Report of the Intergovernmental Panel on Climate Change* 3–32 (2021) doi:10.1017/9781009157896.001.
53. Esquivel-Muelbert, A. *et al.* Compositional response of Amazon forests to climate change. *Global Change Biology* **25**, 39–56 (2019).
54. Li, Y. *et al.* Deforestation-induced climate change reduces carbon storage in remaining tropical forests. *Nat Commun* **13**, 1964 (2022).
55. Kooperman, G. J. *et al.* Forest response to rising CO₂ drives zonally asymmetric rainfall change over tropical land. *Nature Clim Change* **8**, 434–440 (2018).
56. Hubau, W. *et al.* Asynchronous carbon sink saturation in African and Amazonian tropical forests. *Nature* **579**, 80–87 (2020).
57. Brienen, R. J. W. *et al.* Long-term decline of the Amazon carbon sink. *Nature* **519**, 344–348 (2015).
58. Trumbore, S., Brando, P. & Hartmann, H. Forest health and global change. *Science* **349**, 814–818 (2015).
59. Körner, C. A matter of tree longevity. *Science* **355**, 130–131 (2017).
60. Yang, Y. *et al.* Post-drought decline of the Amazon carbon sink. *Nat Commun* **9**, 3172 (2018).
61. Slik, J. W. F. *et al.* Phylogenetic classification of the world’s tropical forests. *Proceedings of the National Academy of Sciences* **115**, 1837–1842 (2018).
62. Fleischer, K. *et al.* Amazon forest response to CO₂ fertilization dependent on plant phosphorus acquisition. *Nat. Geosci.* **12**, 736–741 (2019).
63. Cole, L. E. S., Bhagwat, S. A. & Willis, K. J. Recovery and resilience of tropical forests after disturbance. *Nature Communications* **5**, 3906 (2014).
64. Liu, L. *et al.* Tropical tall forests are more sensitive and vulnerable to drought than short forests. *Global Change Biology* **28**, 1583–1595 (2022).
65. Anderegg, W. R. L. *et al.* Meta-analysis reveals that hydraulic traits explain cross-species patterns of drought-induced tree mortality across the globe. *PNAS* **113**, 5024–5029 (2016).
66. Bittencourt, P. R. L. *et al.* Amazonia trees have limited capacity to acclimate plant hydraulic properties in response to long-term drought. *Global Change Biology* **26**, 3569–3584 (2020).
67. Canadell, J. *et al.* Maximum rooting depth of vegetation types at the global scale. *Oecologia* **108**, 583–595 (1996).
68. Jackson, R. B. *et al.* A global analysis of root distributions for terrestrial biomes. *Oecologia* **108**, 389–411 (1996).
69. Schenk, H. J. & Jackson, R. B. The Global Biogeography of Roots. *Ecological Monographs* **72**, 311–328 (2002).
70. Dittert, K., Wätzel, J. & Sattelmacher, B. Responses of *Alnus glutinosa* to Anaerobic Conditions - Mechanisms and Rate of Oxygen Flux into the Roots. *Plant Biology* **8**, 212–223 (2006).
71. Alvarez-Uria, P. & Körner, C. Low temperature limits of root growth in deciduous and evergreen temperate tree species. *Functional Ecology* **21**, 211–218 (2007).
72. Brunner, I., Herzog, C., Dawes, M. A., Arend, M. & Sperisen, C. How tree roots respond to drought. *Frontiers in Plant Science* **6**, (2015).
73. Bonal, D., Burban, B., Stahl, C., Wagner, F. & Hérault, B. The response of tropical rainforests to drought—lessons from recent research and future prospects. *Annals of Forest Science* **73**, 27–44 (2016).
74. Sankaran, M. Droughts and the ecological future of tropical savanna vegetation. *Journal of Ecology* **107**, 1531–1549 (2019).
75. Mamalakis, A. *et al.* Zonally contrasting shifts of the tropical rain belt in response to climate change. *Nature Climate Change* **11**, 143–151 (2021).
76. Bovolo, C. I. *et al.* The Guiana Shield rainforests—overlooked guardians of South American climate. *Environ. Res. Lett.* **13**, 074029 (2018).

77. van der Ent, R. J., Savenije, H. H. G., Schaeffli, B. & Steele-Dunne, S. C. Origin and fate of atmospheric moisture over continents. *Water Resources Research* **46**, (2010).
78. Zemp, D. C. *et al.* On the importance of cascading moisture recycling in South America. *Atmospheric Chemistry and Physics* **14**, 13337–13359 (2014).
79. Pascale, S., Carvalho, L. M. V., Adams, D. K., Castro, C. L. & Cavalcanti, I. F. A. Current and Future Variations of the Monsoons of the Americas in a Warming Climate. *Curr Clim Change Rep* **5**, 125–144 (2019).
80. Zilli, M. T., Carvalho, L. M. V. & Lintner, B. R. The poleward shift of South Atlantic Convergence Zone in recent decades. *Clim Dyn* **52**, 2545–2563 (2019).
81. Xie, S.-P. *et al.* Global Warming Pattern Formation: Sea Surface Temperature and Rainfall. *Journal of Climate* **23**, 966–986 (2010).
82. Dunning, C. M., Black, E. & Allan, R. P. Later Wet Seasons with More Intense Rainfall over Africa under Future Climate Change. *Journal of Climate* **31**, 9719–9738 (2018).
83. Cook, K. H. & Vizy, E. K. Impact of climate change on mid-twenty-first century growing seasons in Africa. *Clim Dyn* **39**, 2937–2955 (2012).
84. Wunderling, N. *et al.* Recurrent droughts increase risk of cascading tipping events by outpacing adaptive capacities in the Amazon rainforest. *Proceedings of the National Academy of Sciences* **119**, e2120777119 (2022).
85. Staal, A. *et al.* Forest-rainfall cascades buffer against drought across the Amazon. *Nature Climate Change* **8**, 539–543 (2018).
86. Schumacher, D. L., Keune, J., Dirmeyer, P. & Miralles, D. G. Drought self-propagation in drylands due to land–atmosphere feedbacks. *Nat. Geosci.* **15**, 262–268 (2022).
87. Leite-Filho, A. T., Soares-Filho, B. S., Davis, J. L., Abrahão, G. M. & Börner, J. Deforestation reduces rainfall and agricultural revenues in the Brazilian Amazon. *Nat Commun* **12**, 2591 (2021).
88. Hasegawa, T., Fujimori, S., Ito, A., Takahashi, K. & Masui, T. Global land-use allocation model linked to an integrated assessment model. *Science of The Total Environment* **580**, 787–796 (2017).
89. Cai, Y., Judd, K. L., Lenton, T. M., Lontzek, T. S. & Narita, D. Environmental tipping points significantly affect the cost–benefit assessment of climate policies. *Proceedings of the National Academy of Sciences* **112**, 4606–4611 (2015).
90. Estrada, F., Tol, R. S. J. & Botzen, W. J. W. Extending integrated assessment models’ damage functions to include adaptation and dynamic sensitivity. *Environmental Modelling & Software* **121**, 104504 (2019).
91. Yu, Z., Lu, C., Tian, H. & Canadell, J. G. Largely underestimated carbon emission from land use and land cover change in the conterminous United States. *Global Change Biology* **25**, 3741–3752 (2019).
92. Hoek van Dijke, A. J. *et al.* Shifts in regional water availability due to global tree restoration. *Nat. Geosci.* **15**, 363–368 (2022).
93. Ma, L. *et al.* Global rules for translating land-use change (LUH2) to land-cover change for CMIP6 using GLM2. *Geoscientific Model Development* **13**, 3203–3220 (2020).
94. Yu, Z. *et al.* Natural forest growth and human induced ecosystem disturbance influence water yield in forests. *Commun Earth Environ* **3**, 148 (2022).
95. Alves de Oliveira, B. F., Bottino, M. J., Nobre, P. & Nobre, C. A. Deforestation and climate change are projected to increase heat stress risk in the Brazilian Amazon. *Commun Earth Environ* **2**, 1–8 (2021).
96. Funk, C. *et al.* The climate hazards infrared precipitation with stations—a new environmental record for monitoring extremes. *Scientific Data* **2**, 150066 (2015).
97. Jiang, C. & Ryu, Y. Multi-scale evaluation of global gross primary productivity and evapotranspiration products derived from Breathing Earth System Simulator (BESS). *Remote Sensing of Environment* **186**, 528–547 (2016).
98. Zhang, Y. *et al.* Multi-decadal trends in global terrestrial evapotranspiration and its components. *Scientific Reports* **6**, 19124 (2016).
99. Jung, M. *et al.* The FLUXCOM ensemble of global land-atmosphere energy fluxes. *Sci Data* **6**, 74 (2019).
100. Hersbach, H. *et al.* The ERA5 Global Reanalysis. *Quarterly Journal of the Royal Meteorological Society* **245**, 111840 (2020).

101. ESA. GlobCover land-use map. http://due.esrin.esa.int/page_globcover.php (2010).
102. McFarlane, N. Parameterizations: representing key processes in climate models without resolving them. *WIREs Climate Change* **2**, 482–497 (2011).
103. Baker, J. C. A. *et al.* Robust Amazon precipitation projections in climate models that capture realistic land–atmosphere interactions. *Environ. Res. Lett.* **16**, 074002 (2021).
104. Cooper, G. S., Willcock, S. & Dearing, J. A. Regime shifts occur disproportionately faster in larger ecosystems. *Nature Communications* **11**, 1175 (2020).
105. Poorter, L. *et al.* Biomass resilience of Neotropical secondary forests. *Nature* **530**, 211–214 (2016).

Supplementary Information

Multi-fold increase in rainforests tipping risk beyond 1.5-2°C warming

Chandrakant Singh^{1,2,*}, Ruud van der Ent³, Ingo Fetzer^{1,2}, Lan Wang-Erlandsson^{1,2}

¹Stockholm Resilience Centre, Stockholm University, Stockholm, Sweden

²Bolin Centre for Climate Research, Stockholm University, Stockholm, Sweden

³Department of Water Management, Faculty of Civil Engineering and Geosciences, Delft University of Technology, Delft, The Netherlands

*Corresponding author; E-mail: chandrakant.singh@su.se

Content

Supplementary Methods	2
Calculating root zone storage capacity (S_r)	2
Supplementary Figures	4
Supplementary Figure 1 Root zone storage capacity (S_r) and extent of forest ecosystems	4
Supplementary Figure 2 Distribution of empirical- vs CMIP6-derived root zone storage capacity (S_r) for South America	5
Supplementary Figure 3 Distribution of empirical- vs CMIP6-derived root zone storage capacity (S_r) for Africa	6
Supplementary Figure 4 Forest-savanna transition correction based on precipitation and precipitation seasonality under the current climate (empirical; 2001-2012)	7
Supplementary Figure 5 State of the tropical forests under different SSP scenarios (2086-2100) w.r.t current climate (empirical; 2001-2012)	8
Supplementary Figure 6 Extent of forest transitions under different SSP scenarios (2086-2100) w.r.t current climate (empirical; 2001-2012)	9
Supplementary Figure 7 Exemplifying the methodological framework for projecting the future transitions in the tropical forests (by the end of the 21st century) based on the 'Australian Community Climate and Earth System Simulator coupled model (ACCESS-CM2)'	10
Supplementary Figure 8 Comparing the forest transitions under different SSP scenarios	11
Supplementary Figure 9 State of the tropical forests under different SSP scenarios (2086-2100) w.r.t current climate (CMIP6-historical; 2000-2014)	12
Supplementary Figure 10 Extent of forest transitions under different SSP scenarios (2086-2100) w.r.t current climate (CMIP-historical; 2000-2014)	13
Supplementary Figure 11 Comparing hydroclimatic changes between current and future climate for forest-savanna transition regions	14
Supplementary Figure 12 Comparing hydroclimatic changes between current and future climate for forests' that transition to a more water-stressed state	15
Supplementary Figure 13 Comparing hydroclimatic changes between current and future climate for forests' that revert to a less water-stressed state	16
Supplementary Figure 14 Comparing forest-savanna transitions with prescribed land-use in ESMs	17

Supplementary Figure 15 Comparing forests that transition to a more water-stressed state with prescribed land-use in ESMs	18
Supplementary Figure 16 Comparing forests that revert to a less water-stressed state with prescribed land-use in ESMs.....	19
Supplementary Figure 17 Analysing and comparing (extreme value) forest-savanna transitions with prescribed land-use in ESMs	20
Supplementary Figure 18 Sensitivity analysis with lower root zone storage capacity (S_r) thresholds.....	21
Supplementary Figure 19 Sensitivity analysis with higher root zone storage capacity (S_r) thresholds.....	22
Supplementary Figure 20 Sensitivity analysis with lower forest-savanna transition threshold	23
Supplementary Figure 21 Sensitivity analysis with higher forest-savanna transition threshold.....	25
Supplementary Figure 22 Comparing root zone storage capacity (S_r) based on daily and monthly estimates of precipitation (P) and evaporation (E) (both empirical; 2001-2012) for South America and Africa.....	26
Supplementary Tables	27
Supplementary Table 1 Overview of analysed Earth System Models (ESMs).....	27
Supplementary Table 2 Citations for CMIP6 datasets used in this study	29
Supplementary References	35

Supplementary Methods

Calculating root zone storage capacity (S_r). We adopted the root zone storage capacity (S_r) calculation method from ref.¹. Here, we first calculate the daily water deficit ($D(t)$) using daily estimates of precipitation ($P(t)$) and evaporation ($E(t)$):

$$D(t) = E(t) - P(t) \quad (1)$$

Where t denotes the day count since the start of the simulation. The simulation for each grid cell starts in the month with the highest mean monthly precipitation (2001-2012) and runs for a whole year.

Since the 6th Coupled Model Intercomparison Project (CMIP6; for the CMIP6-historical and -SSP estimates, the timeframe considered are 2000-2014 and 2086-2100, respectively) doesn't have daily estimates of evaporation and precipitation for all Earth System Models (ESMs), we directly use:

$$D(t) = E(t_{monthly}) - P(t_{monthly}) \quad (2)$$

Where $t_{monthly}$ denotes the month count since the start of the simulation. The rest of the steps below remain the same for both empirical and model-estimated datasets.

Next, we calculate the accumulated deficit $D_a(t+1)$ at each one-day (one-month for ESMs) timestep for one year such that it is either equal to or more than the deficit of the previous timestep. However, this value is never less than zero since we assume the excess precipitation to run off as streamflow or groundwater recharge using:

$$D_a(t+1) = \max\{0, D(t) + D(t+1)\} \quad (3)$$

This analysis assumes that vegetation adapts and responds to the most critical dry periods it has experienced over the year², therefore we compute the largest accumulated deficit per year ($D_{a,y}$) by:

$$D_{a,y} = \max\{D_a(t+1)\} \quad t = 1 : n-1 \quad (4)$$

This paper is a non-peer reviewed preprint submitted to EarthArXiv.

Where n equals the number of days (number of months for CMIP6 datasets) in year y . Since this simulation is run for a whole year using precipitation and evaporation estimates, this mass-balance methodology does consider actual seasonal dynamics of precipitation (incoming moisture flux) and evaporation (outgoing moisture fluxes, including evaporation from soil moisture, interception, transpiration and open water; see methods) at temporal timescales.

Although different terrestrial ecosystems (e.g., forest, savanna and grasslands) adapt to different drought return periods²⁻⁴. For this study, we use a uniform 20-year drought return period to avoid any artificially introduced transitions between different ecosystems. This we analyse using on the Gumbel extreme value distribution⁵ and apply it to normalise all $D_{a,y}$. The Gumbel distribution ($F(x)$) is given by:

$$F(x) = \exp \left[-\exp \left[-\frac{(x - \mu)}{\alpha} \right] \right] \quad (5)$$

Where μ and α are the location and scale parameters, respectively. We calculate this using the python package 'skextremes'⁶:

$$S_r = D_{a,y} + K \times \sigma_{n-1} \quad (6)$$

where K is the frequency factor given by:

$$K = \frac{y_t - y_n}{S_n} \quad (7)$$

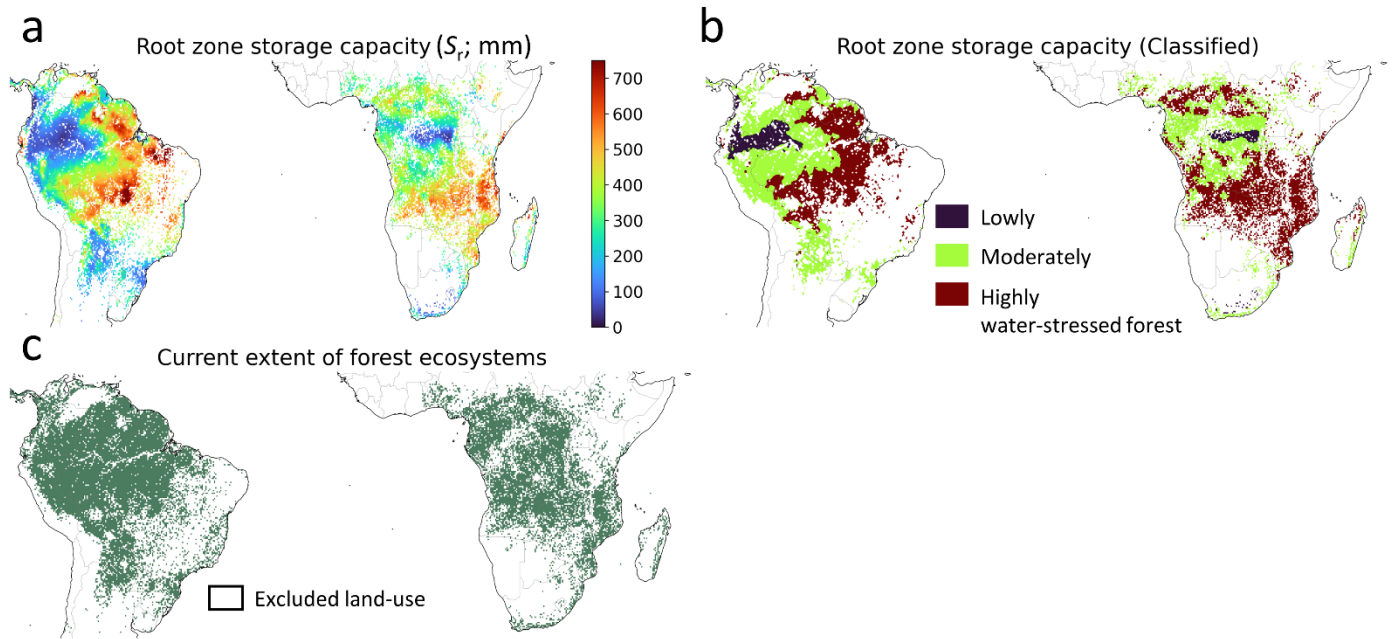
And y_t is the reduced variate given by:

$$y_t = - \left[\ln \left[\ln \left(\frac{T}{T-1} \right) \right] \right] \quad (8)$$

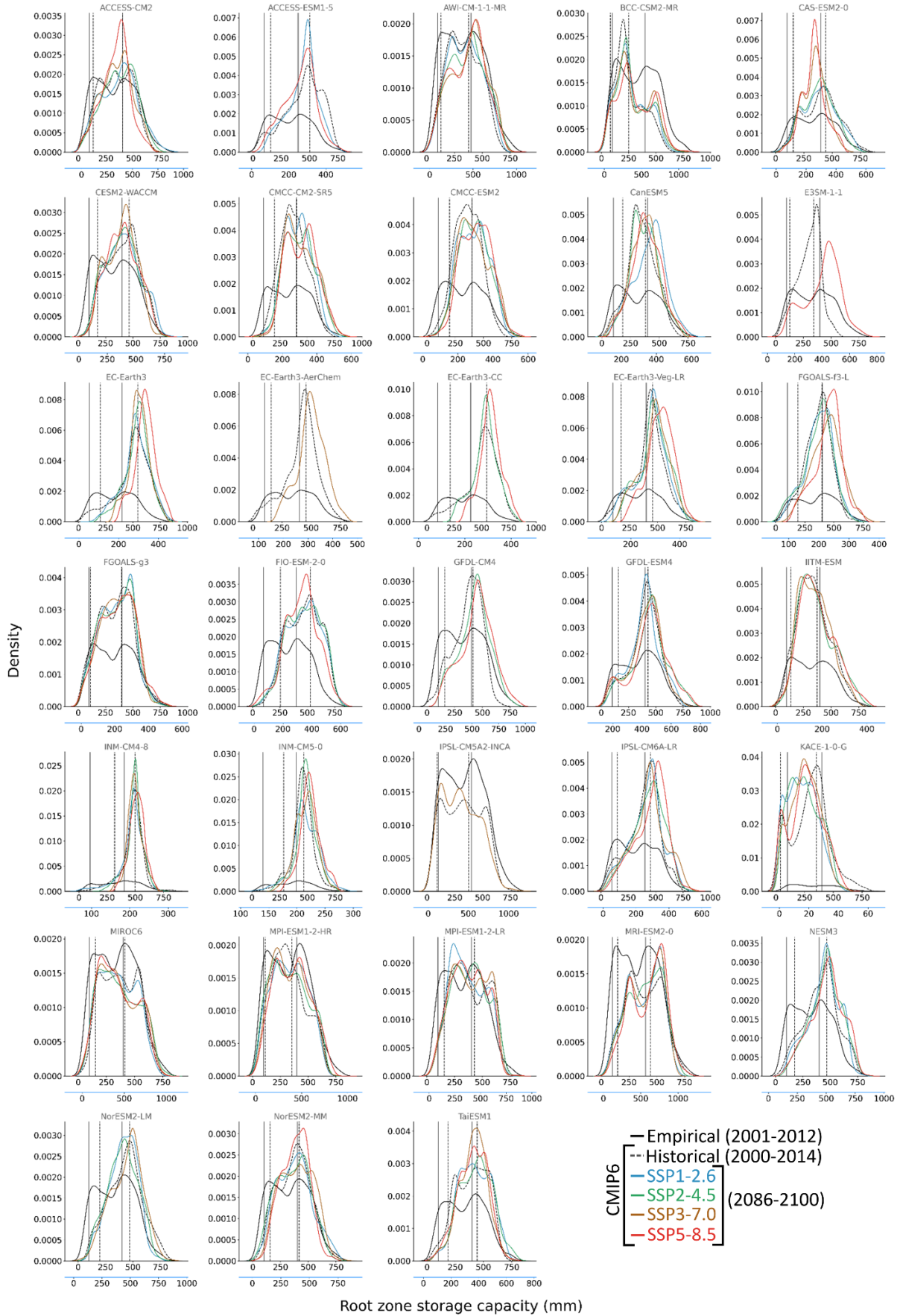
Where T is the drought return period (i.e., 20 years used in this study), $D_{a,y}$ is the mean annual accumulated deficit for the years 2001-2012 (2000-2014 for CMIP6-historical and 2086-2100 for CMIP6-SSPs), σ_{n-1} is the standard deviation of the sample. Also, y_n is the reduced mean and S_n is the reduced standard deviation, which for $n = 11$ years (since we are calculating S_r in a hydrological year, we therefore lose one year) is equal to 0.4996 and 0.9676, respectively; and 0.5100 and 1.0095 for $n = 14$ years, respectively⁵.

We later compare the S_r estimates derived from daily and monthly empirical estimates (Eq. 1 and 2) in Supplementary Figure 22 to evaluate uncertainty.

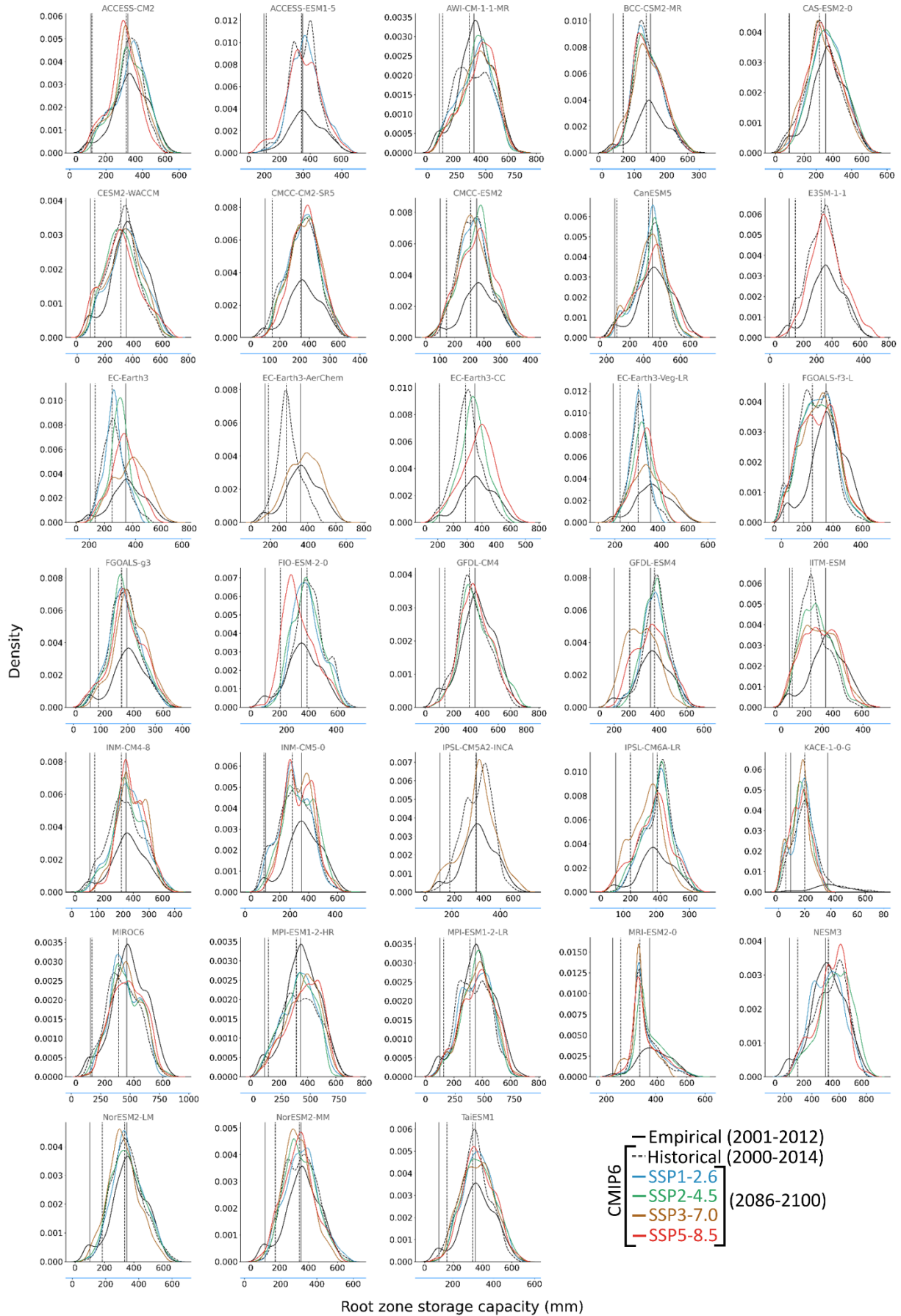
Supplementary Figures



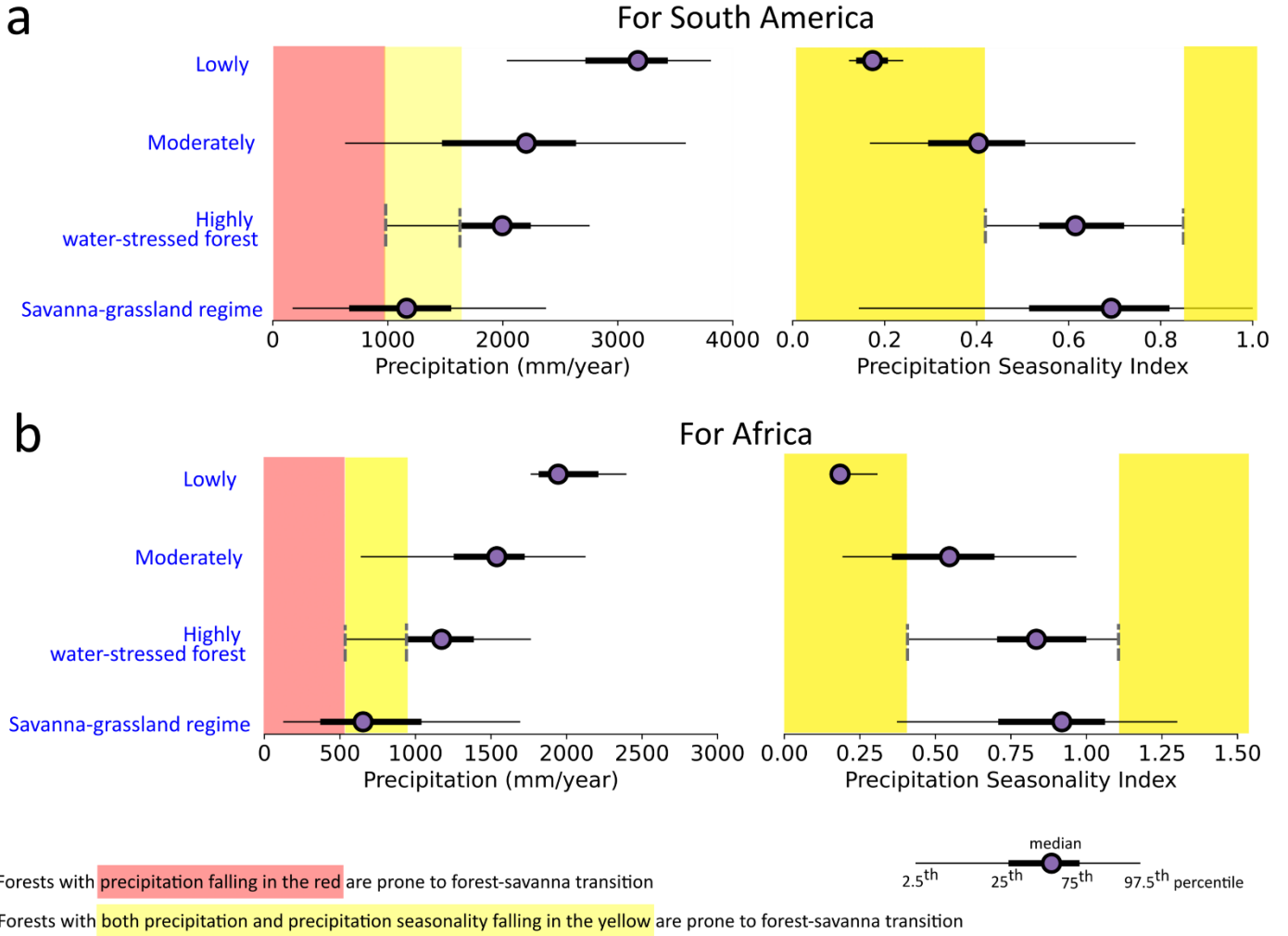
Supplementary Figure 1 | Root zone storage capacity (S_r) and extent of forest ecosystems. (a) Root zone storage capacity (S_r) based on empirical estimates of precipitation and evaporation (2001-2012). (b) Root zone storage capacity (S_r)-based classification of forest ecosystems (see methods). (c) This study's extent of tropical forests is based on the Global landcover classification – Globcover⁷.



Supplementary Figure 2 | Distribution of empirical- vs CMIP6-derived root zone storage capacity (S_r) for South America. Solid vertical lines represent lower and upper S_r threshold, whereas dotted vertical lines represent percentile-equivalent lower and upper S_r threshold based on bias correction (Figure 1a,b and Supplementary Table 1; see methods). The top x-axis (in black) is for empirical S_r estimates, whereas the bottom x-axis (in blue) is for CMIP6 S_r estimates.

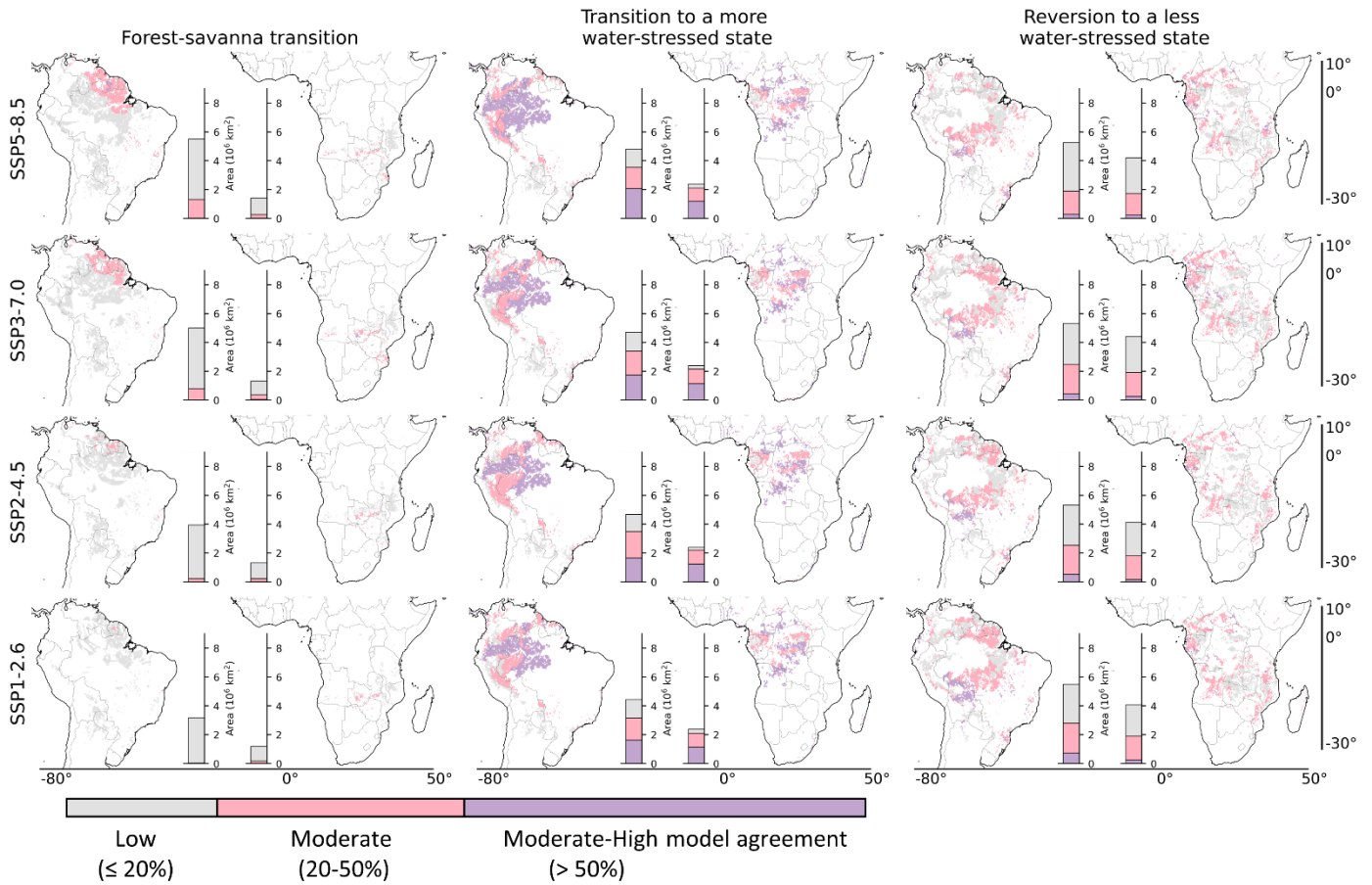


Supplementary Figure 3 | Distribution of empirical- vs CMIP6-derived root zone storage capacity (S_r) for Africa. Same as Supplementary Figure 2, but for Africa.

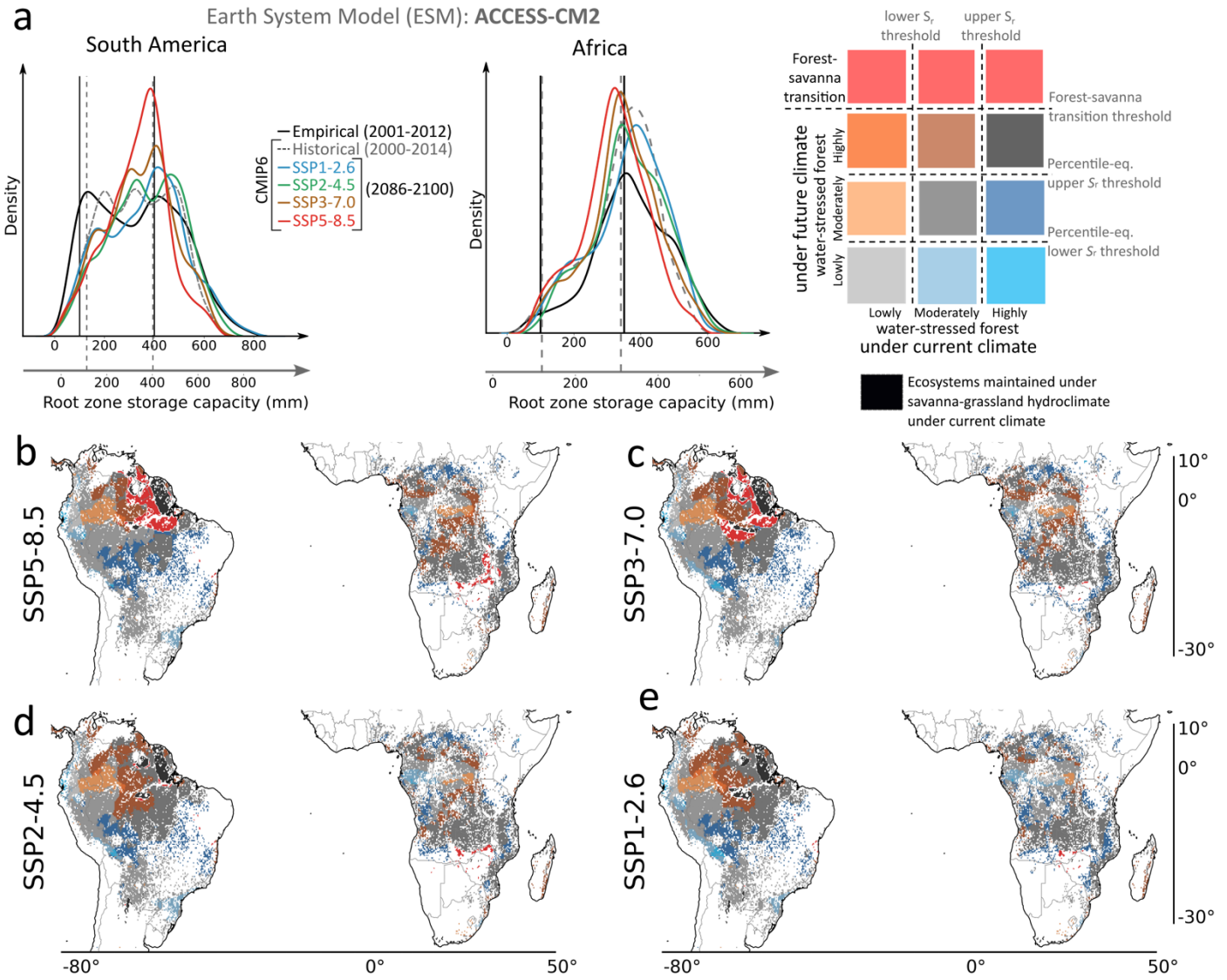


Supplementary Figure 4 | Forest-savanna transition correction based on precipitation and precipitation seasonality under the current climate (empirical; 2001-2012). Dashed lines define the quantitative estimate of the threshold (for more details, refer to the methods and Figure 1). Precipitation seasonality index is calculated using ref.⁸

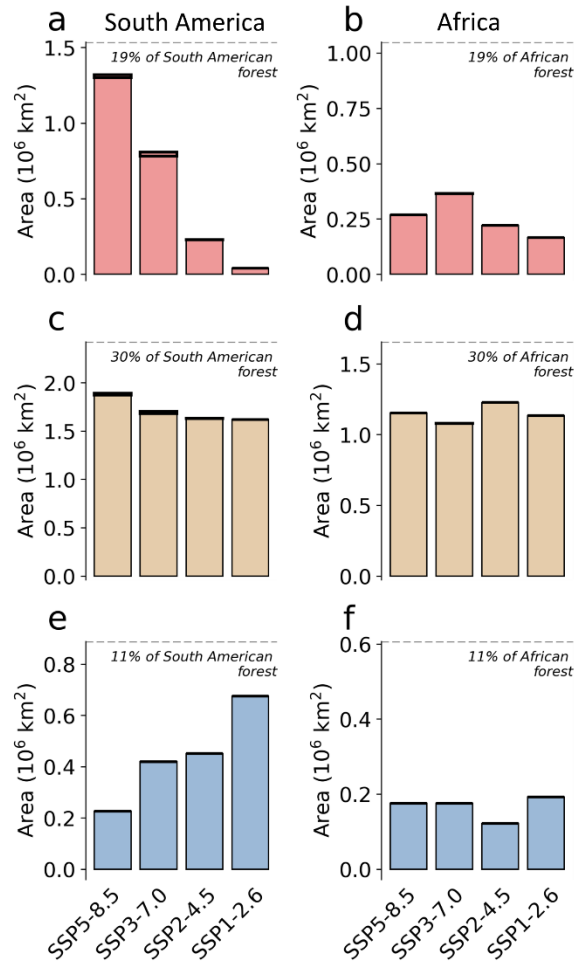
$\left(\frac{1}{R_i} \sum_{n=1}^{12} \left| X_{in} - \frac{R_i}{12} \right| \right)$. Here, R_i and X_{in} denote the total annual precipitation and monthly precipitation for the month n , respectively.



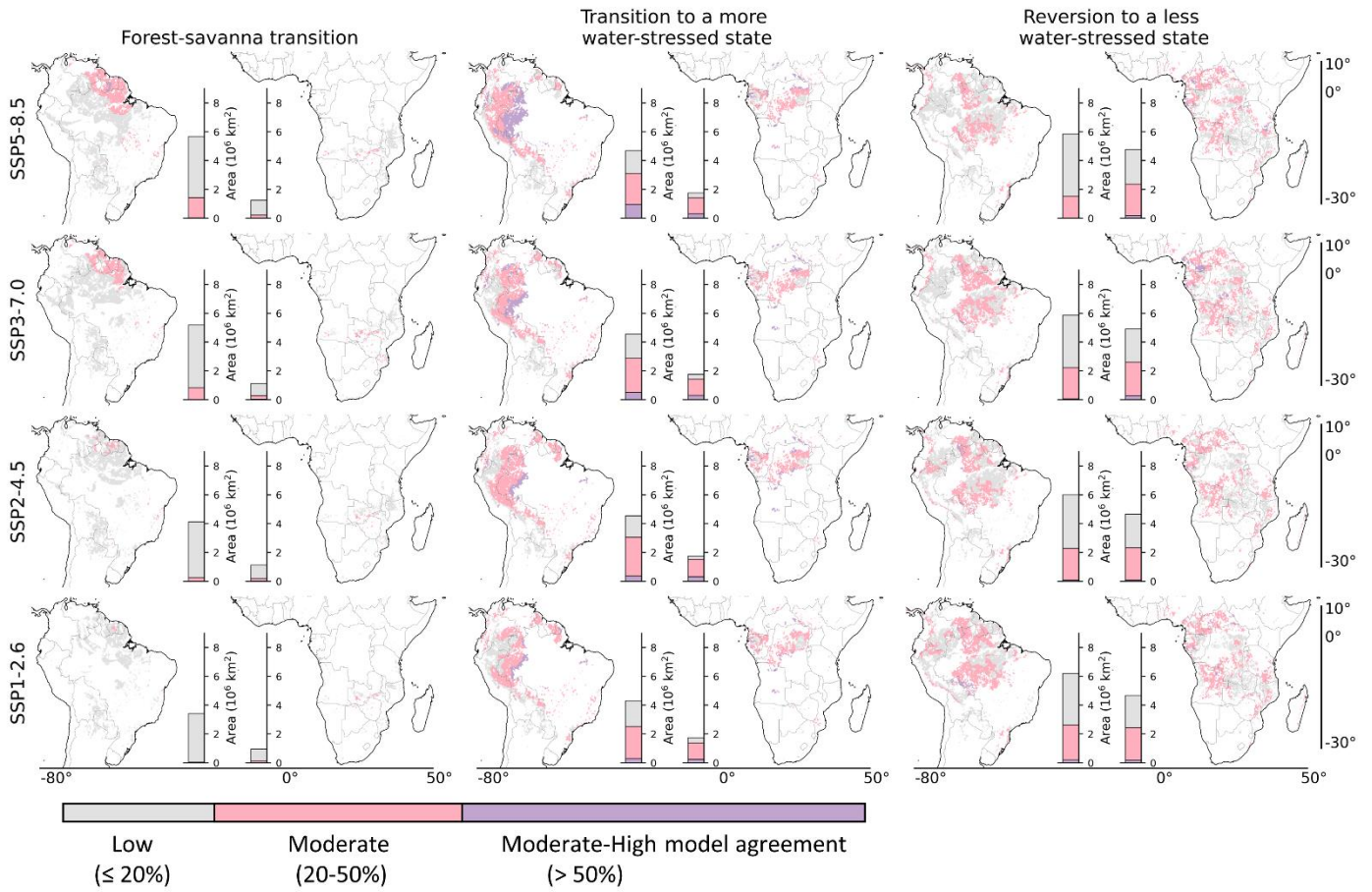
Supplementary Figure 6 | Extent of forest transitions under different SSP scenarios (2086-2100) w.r.t current climate (empirical; 2001-2012). Here, the transitions are derived based on the state of the forests under the current climate (empirical; 2001-2012). Bar plots within each subplot – left for South America and right for Africa – correspond to the synthesised area of model agreement. Synthesis for this figure is provided in Figures 2 and 3.



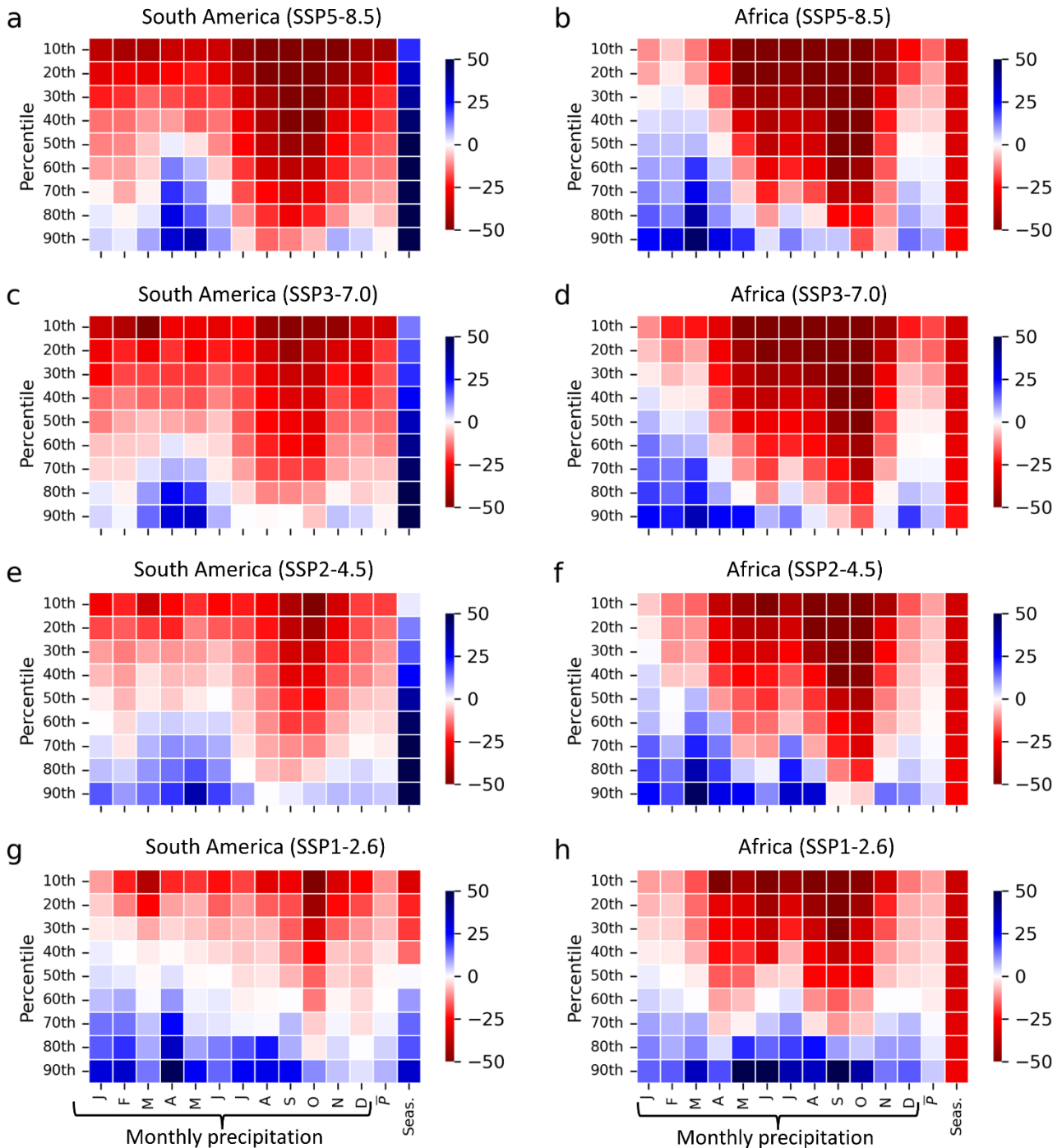
Supplementary Figure 7 | Exemplifying the methodological framework for projecting the future transitions in the tropical forests (by the end of the 21st century) based on the 'Australian Community Climate and Earth System Simulator coupled model (ACCESS-CM2)'. (a) Frequency density distribution of empirical (based on empirical P and E estimates) and CMIP6-derived S_r (based on P and E estimates from ACCESS-CM2 simulations) for South America and Africa. Based on empirical S_r classification, the solid vertical lines mark the lower (100 mm for both South America and Africa) and upper (400 mm for South America and 350 mm for Africa) S_r thresholds. Whereas dotted vertical lines demarcate the lower (116.58 mm for South America and 121.11 mm for Africa) and upper (409.90 mm for South America and 310.66 mm for Africa) percentile-equivalent S_r thresholds for CMIP6-historical (i.e., 2000-2014) models. We analyse forest-savanna transitions based on Supplementary Figure 4. **(b-e)** Forests classification and transitions under different SSP scenarios, based on the comparison between empirical and CMIP6-SSPs (i.e., 2086-2100) derived forest classes (legend in the top-right corner). The white regions correspond to excluded landcover, including water and human-influenced land use (Supplementary Figure 1c).



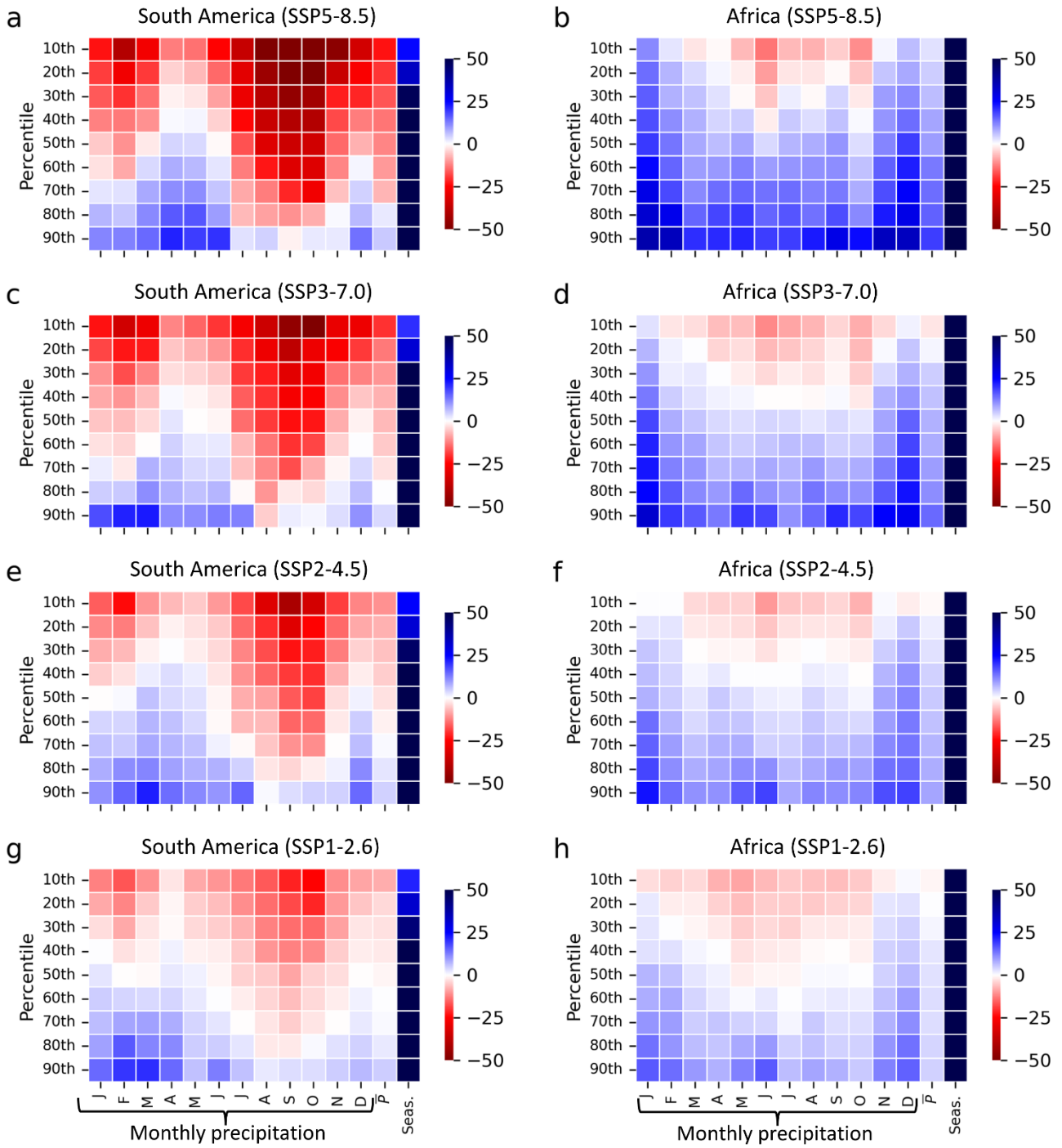
Supplementary Figure 8 | Comparing the forest transitions under different SSP scenarios. Same as Figure 2, quantifying (a,b) forest-savanna transition, (c,d) forests' that transition to a more water-stressed state and (e,f) revert to a less water-stressed state for South America (total forest area $8.08 \times 10^6 \text{ km}^2$) and Africa (total forest area $5.52 \times 10^6 \text{ km}^2$). However, the model agreement is >20% for the forest-savanna transition, and for the other two transitions, the model agreement is >50%. These quantifications show the forests' state changes based on empirical-current (2001-2012) and future (2086-2100) climate conditions. For each transition, the total area of spatial overlap with other transitions under the same SSP scenario is highlighted with thick black bars.



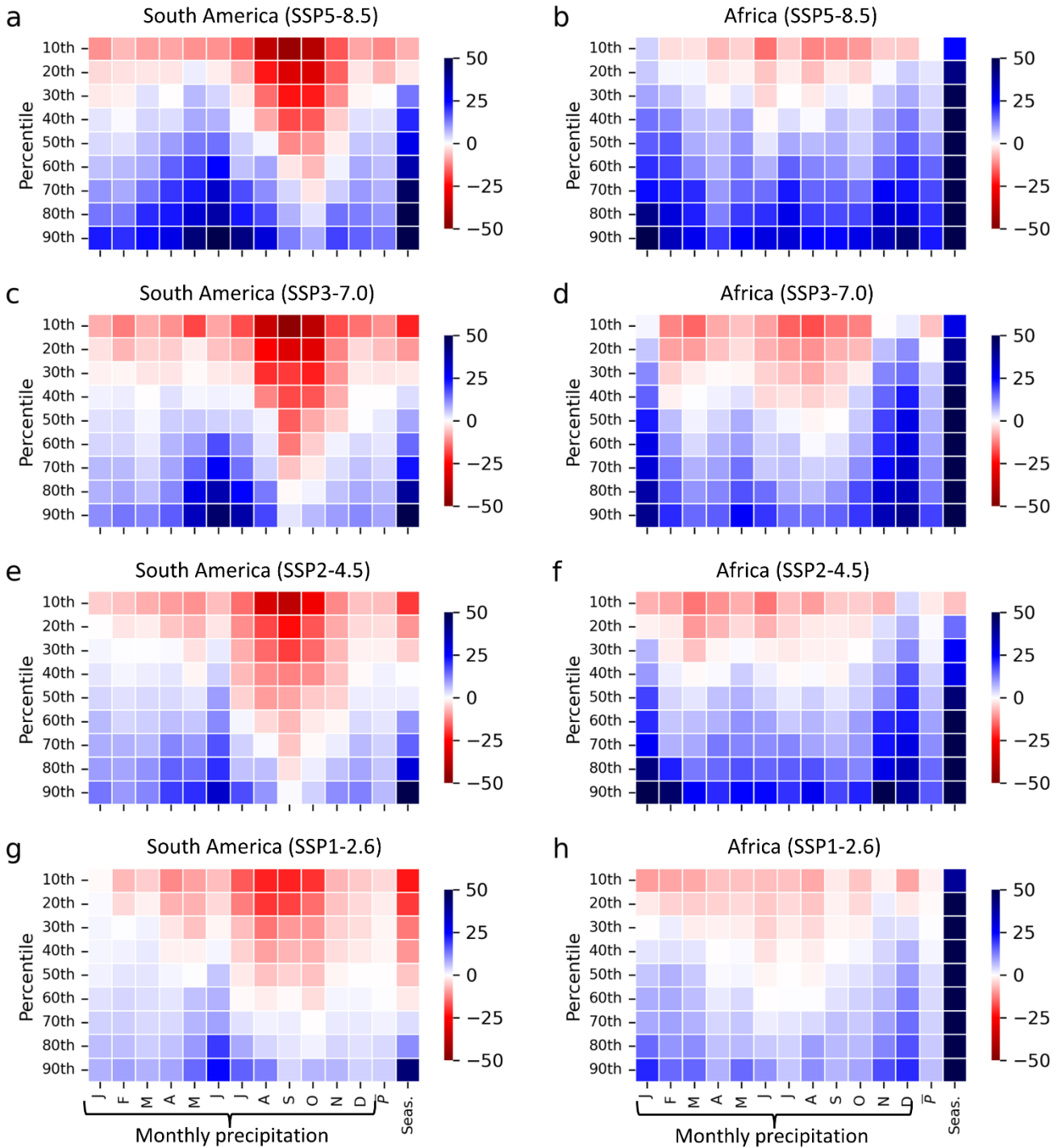
Supplementary Figure 10 | Extent of forest transitions under different SSP scenarios (2086-2100) w.r.t current climate (CMIP-historical; 2000-2014). Same as Figure 6, but compared to CMIP-historical estimates (2000-2014).



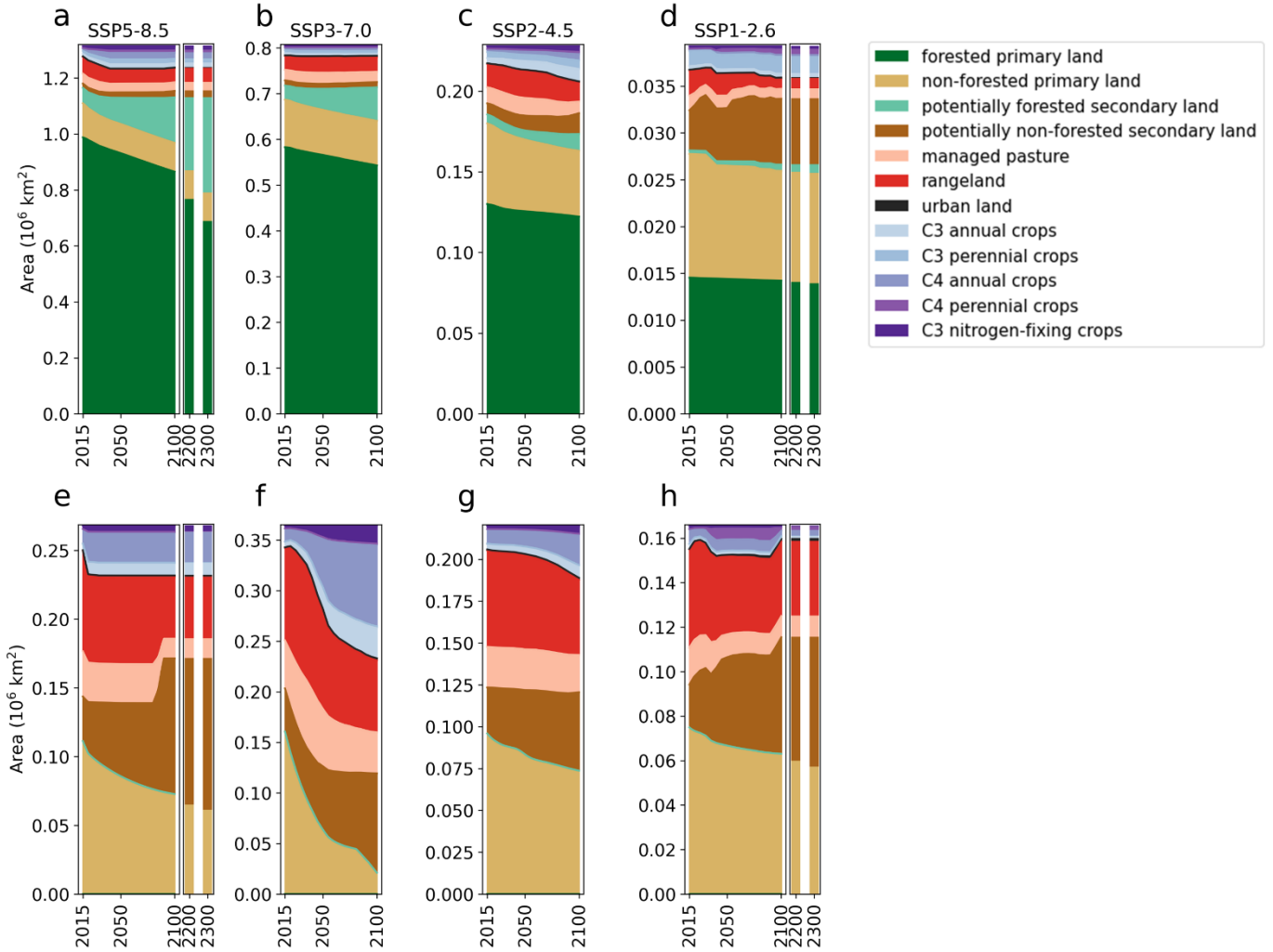
Supplementary Figure 11 | Comparing hydroclimatic changes between current and future climate for forest-savanna transition regions. The extent of forest-savanna transition can be referred from Figure 3. Since there is considerable variability between empirical and CMIP6-model estimates, we directly compare current (CMIP6-historical; 2000-2014) hydroclimate with the future (CMIP6-SSPs; 2086-2100) using estimates from the ESMs. Here, we focus on monthly precipitation, mean annual precipitation (\bar{P}) and precipitation seasonality (Seas.). The percentile is calculated across different ESMs. The colour bar represents the % change in variables with respect to the current climate (2000-2014).



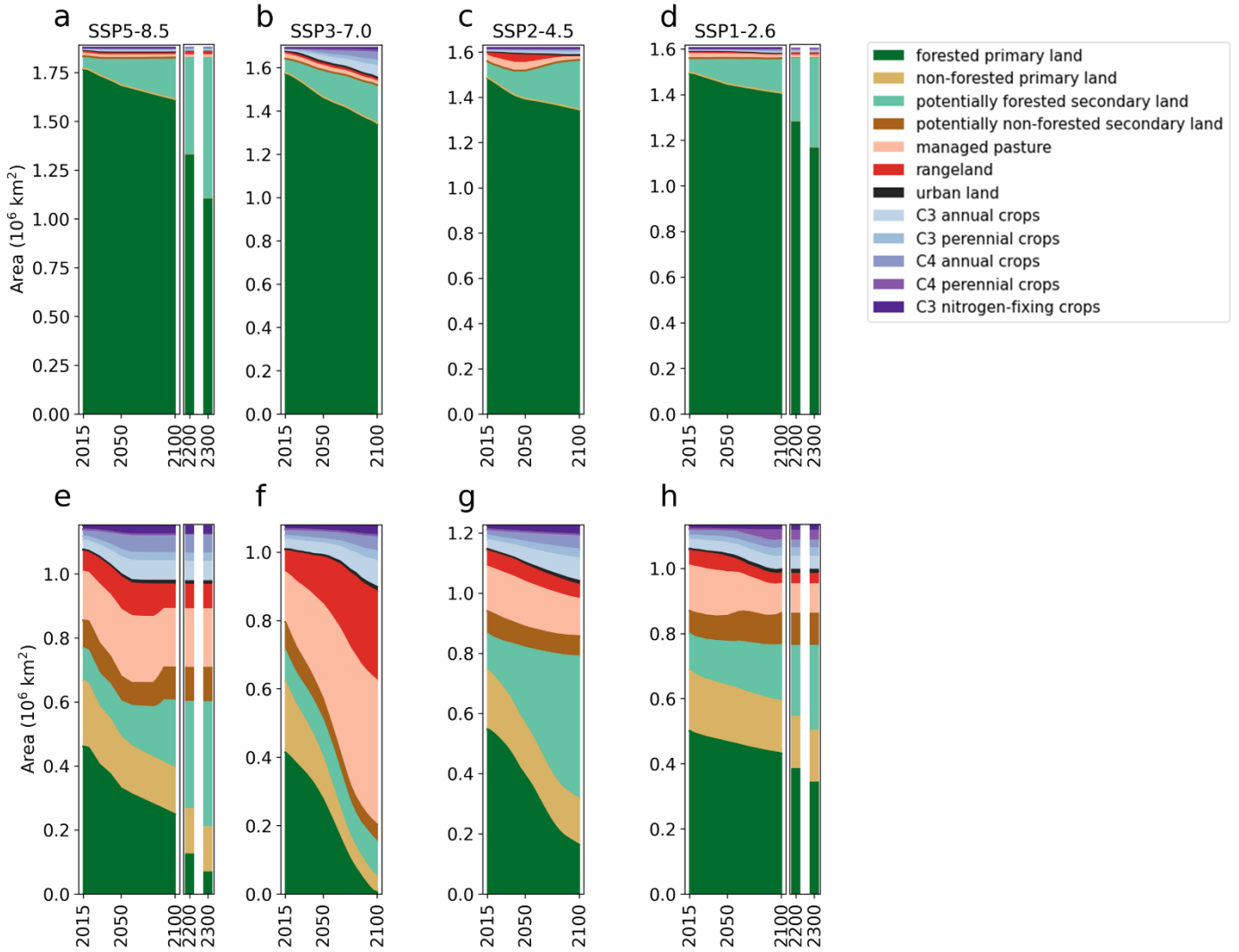
Supplementary Figure 12 | Comparing hydroclimatic changes between current and future climate for forests' that transition to a more water-stressed state. Same as Supplementary Figure 11, but for forest ecosystems that transition to a 'more' water-stressed state.



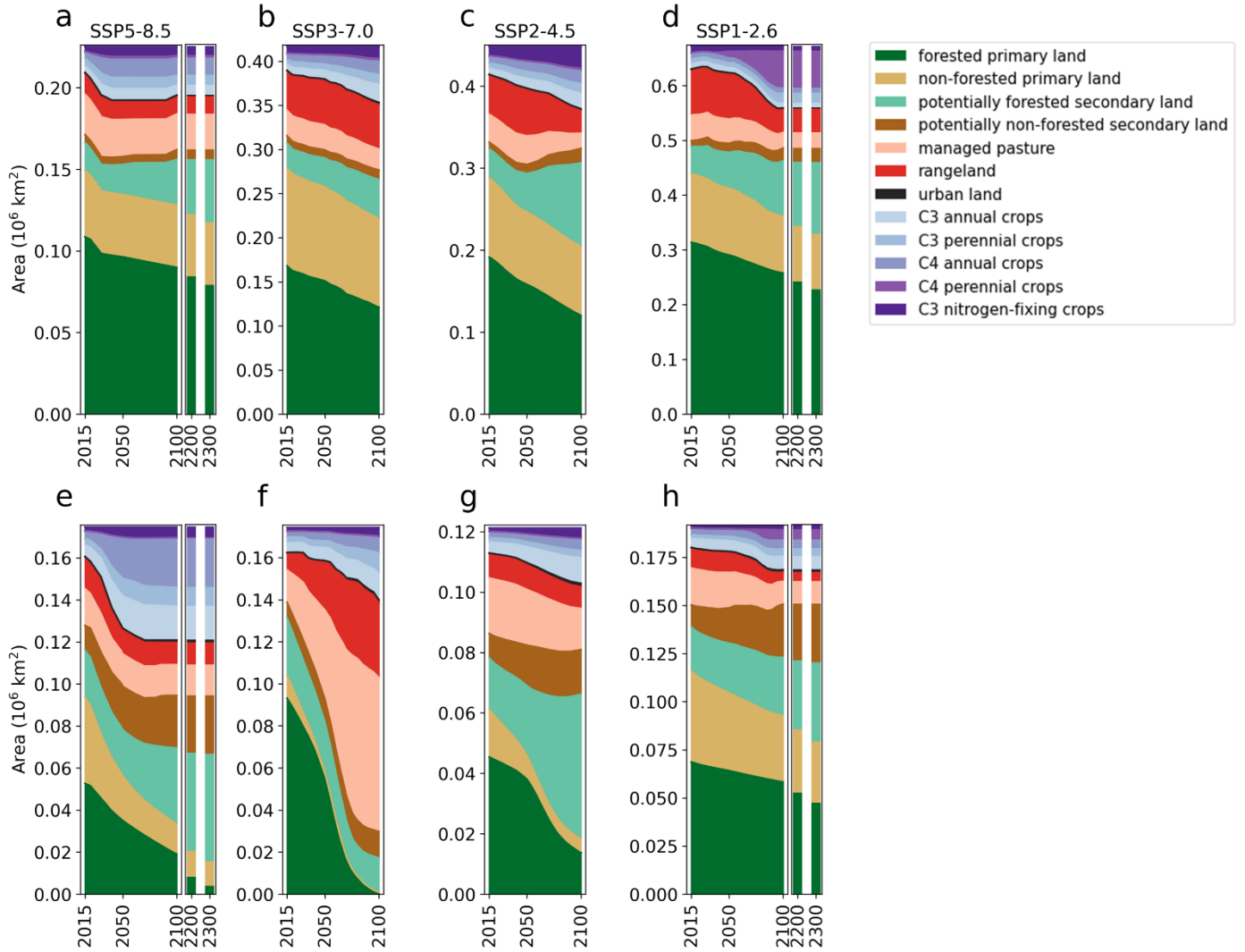
Supplementary Figure 13 | Comparing hydroclimatic changes between current and future climate for forests' that revert to a less water-stressed state. Same as Supplementary Figure 11, but for forest ecosystems that revert to a 'less' water-stressed state.



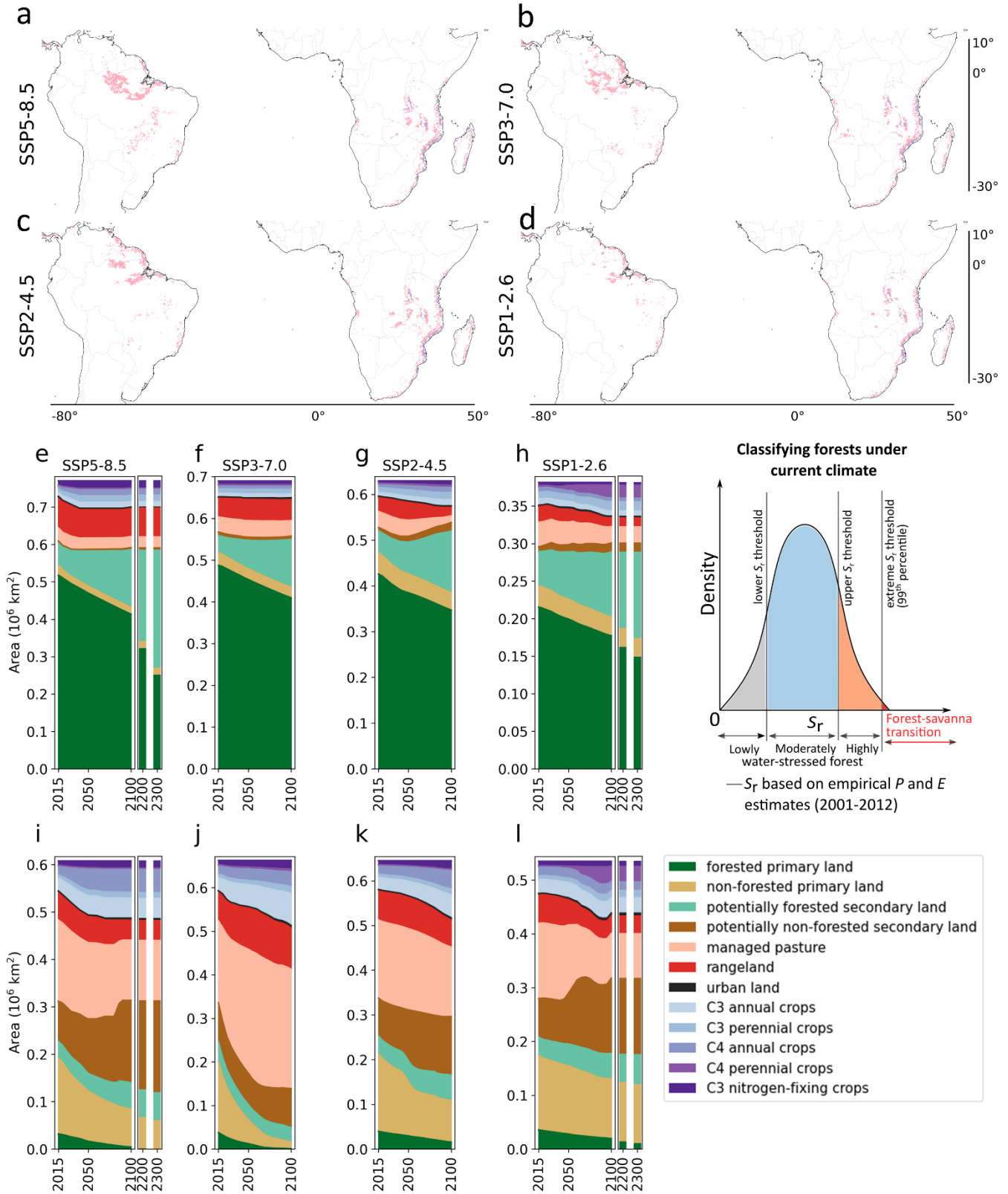
Supplementary Figure 14 | Comparing forest-savanna transitions with prescribed land-use in ESMs. Here, we compare Integrated Assessment Models (IAMs) derived land-use (also referred to as 'land-use harmonisation'⁹) with projected forest-savanna transitions (extent of transition defined in Figure 3). We analyse the land-use between 2015-2100 and the median between 2186-2200 and 2286-2300 for (a-d) South America and (e-h) Africa. Here, 'primary' land-use refers to the regions that have never been impacted by human influence since the start of the simulation. Note that extended prescribed harmonised land-use data (2100-2300) is only available for SSP5-8.5 and SSP1-2.6, and therefore is not analysed for the other two SSP scenarios.



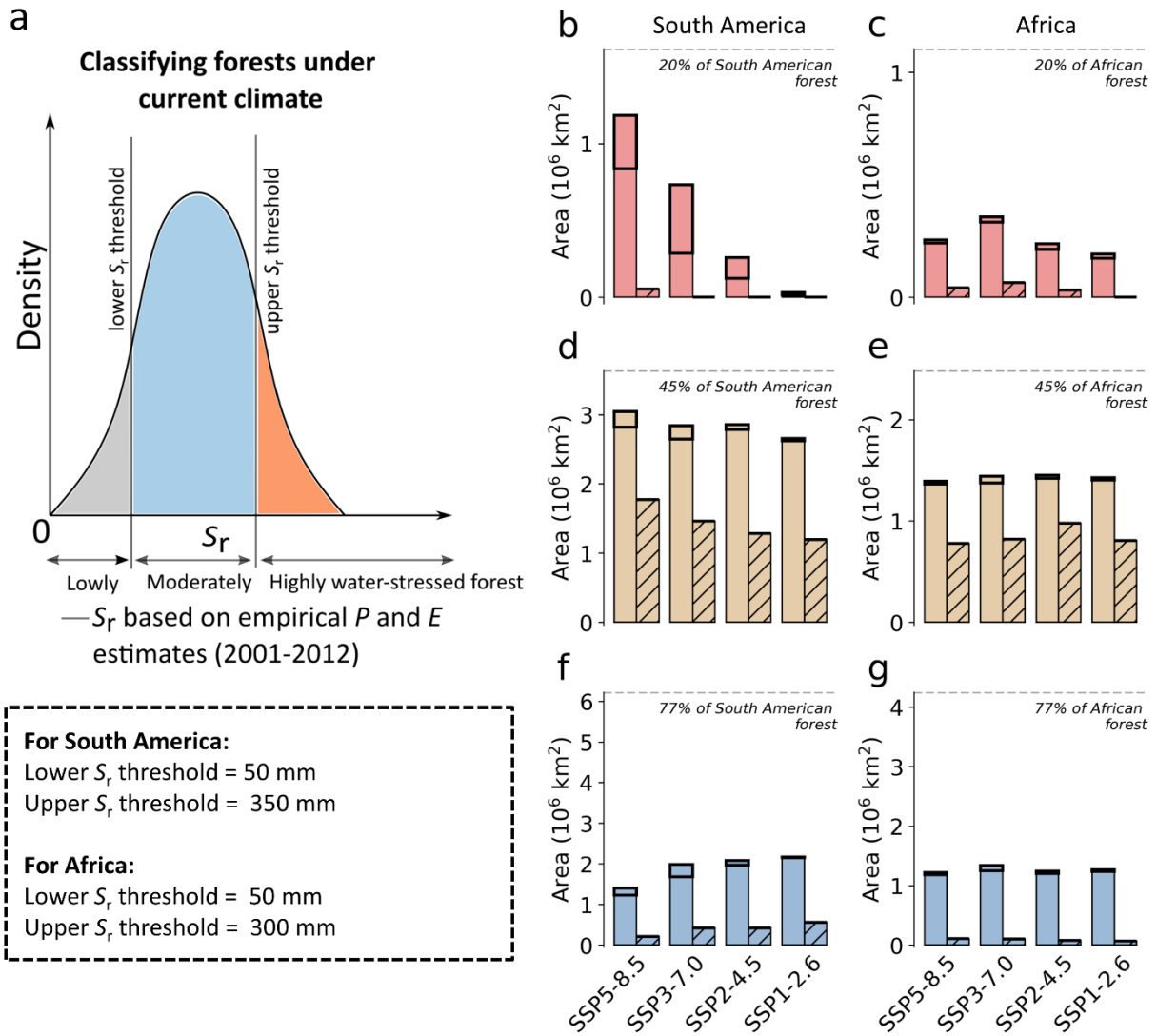
Supplementary Figure 15 | Comparing forests that transition to a more water-stressed state with prescribed land-use in ESMs. Same as Supplementary Figure 14, but for the forest that transition to a more water-stressed state.



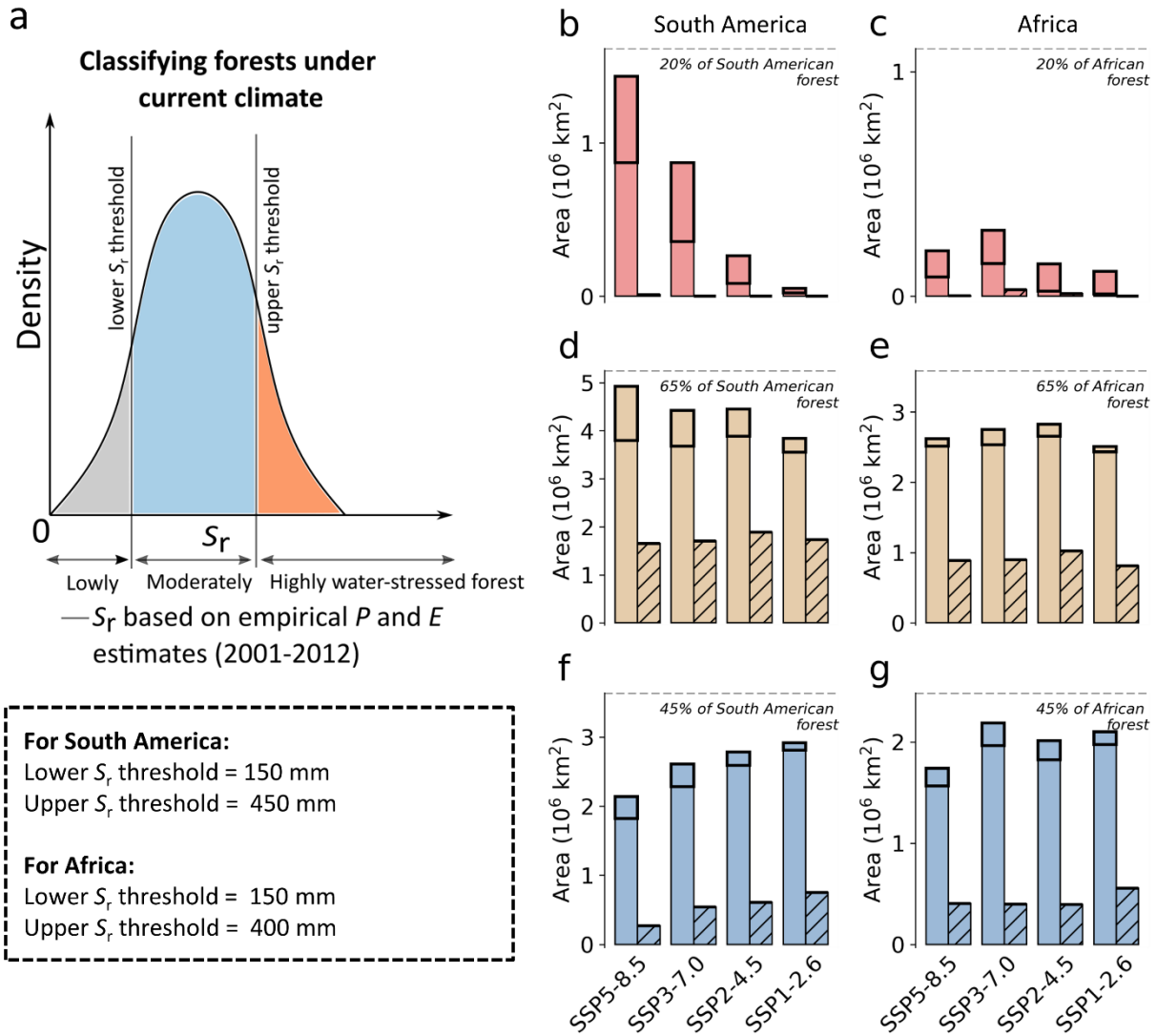
Supplementary Figure 16 | Comparing forests that revert to a less water-stressed state with prescribed land-use in ESMs. Same as Supplementary Figure 14, but for forests that transition to a less water-stressed state.



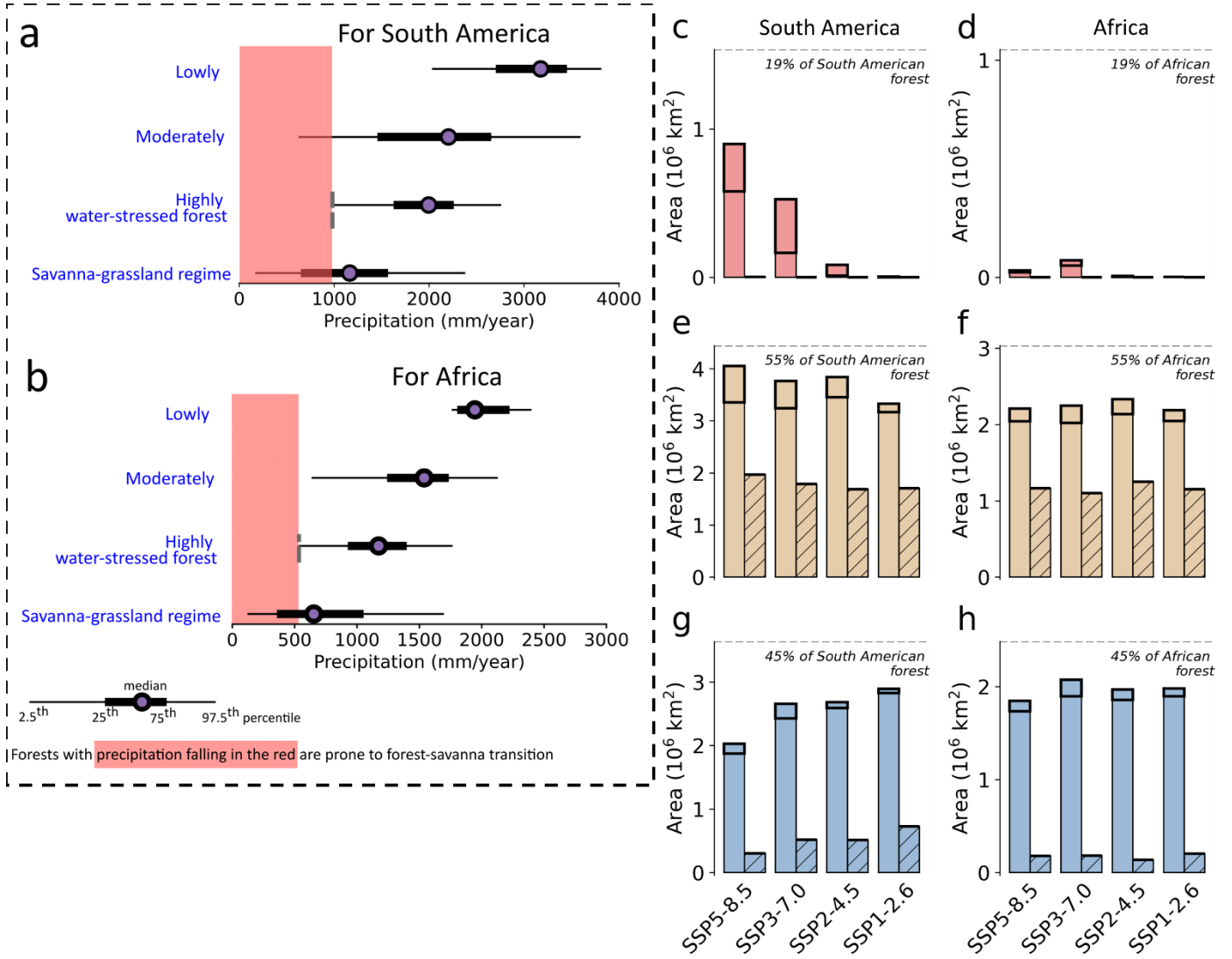
Supplementary Figure 17 | Analysing and comparing (extreme value) forest-savanna transitions with prescribed land-use in ESMs. Considering forest-savanna transition thresholds defined in Figure 4, here we additionally assumed that regions that exceed the 99th percentile S_r are also prone to a forest-savanna transition. (a-d) These additional regions (excluding those already defined in Figure 3) are evaluated using bias-corrected values for all ESMs under different SSP scenarios (same as Figure 1). (e-l) Same as Supplementary Figure 14, but only for the additional regions in a-d (see methods for more details). These additional transition regions are not included in the analyses presented in the Figure 2 and 3.



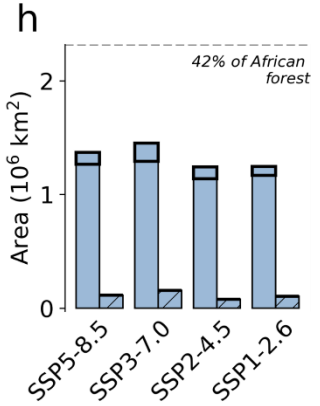
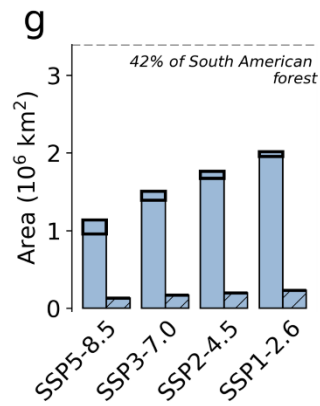
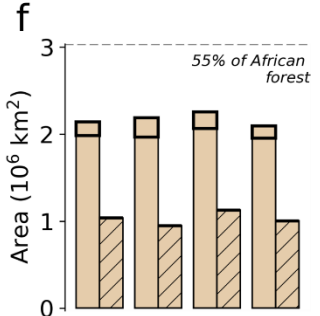
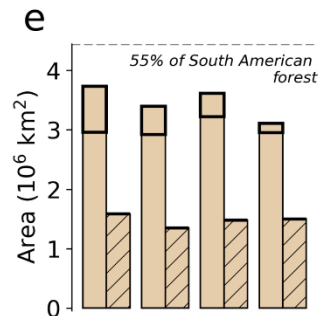
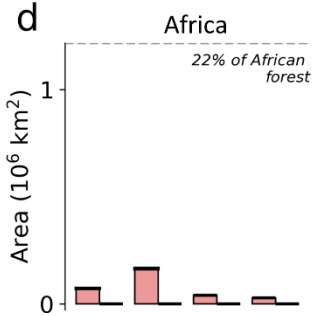
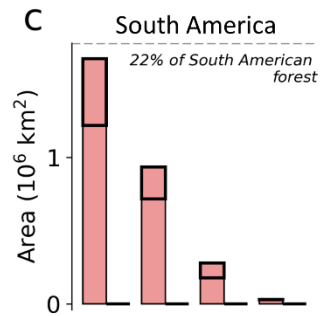
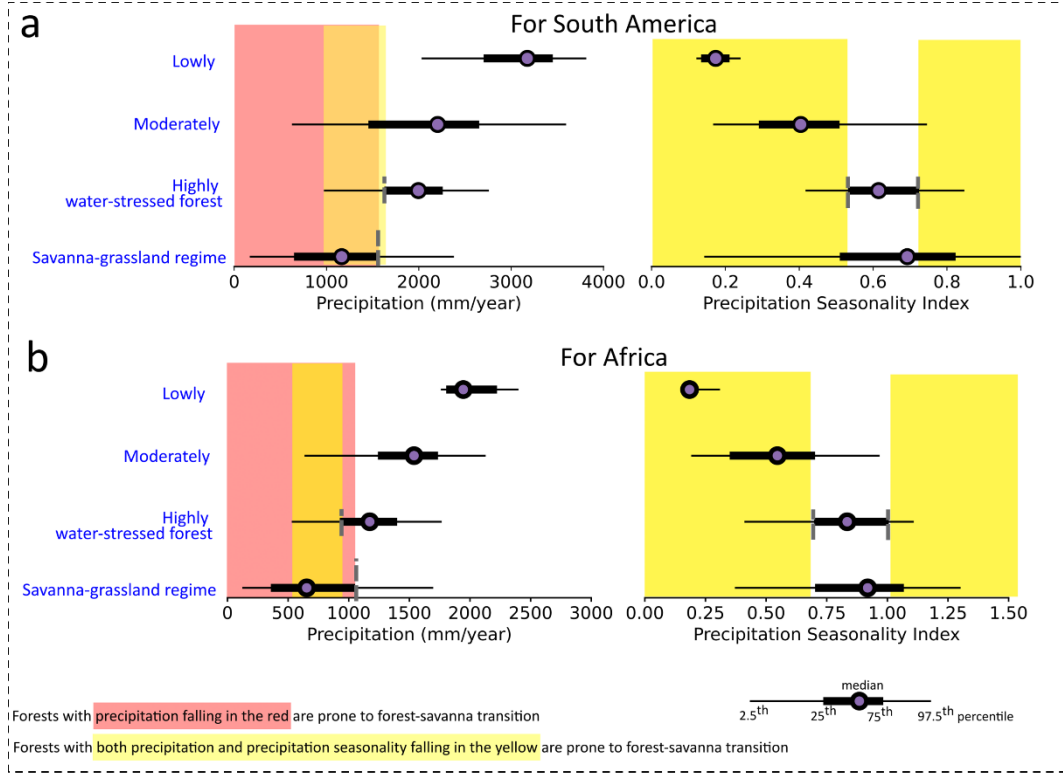
Supplementary Figure 18 | Sensitivity analysis with lower root zone storage capacity (S_r) thresholds. (a) We decreased the upper and lower S_r threshold for South America and Africa for this sensitivity analysis. Here, we quantify (b,c) forest-savanna transition, (d,e) forest ecosystems' that transition to a more water-stressed state and (f,g) revert to a less water-stressed state for South America (total forest area 8.08×10^6 km²) and Africa (total forest area 5.52×10^6 km²), respectively. For the analysis above, transitions are calculated for pixels with model agreement >20% (plain bar plot) and > 50% (hatched bar plot). These quantifications show changes to the forests' state based on empirical-current (2001-2012) and future (2086-2100) climate conditions. The total area of spatial overlap with other transitions under the same SSP scenario and model agreement is highlighted with thick black bars.



Supplementary Figure 19 | Sensitivity analysis with higher root zone storage capacity (S_r) thresholds. Same as Supplementary Figure 18, but for this sensitivity analysis, (a) we increased the upper and lower S_r threshold for South America and Africa.

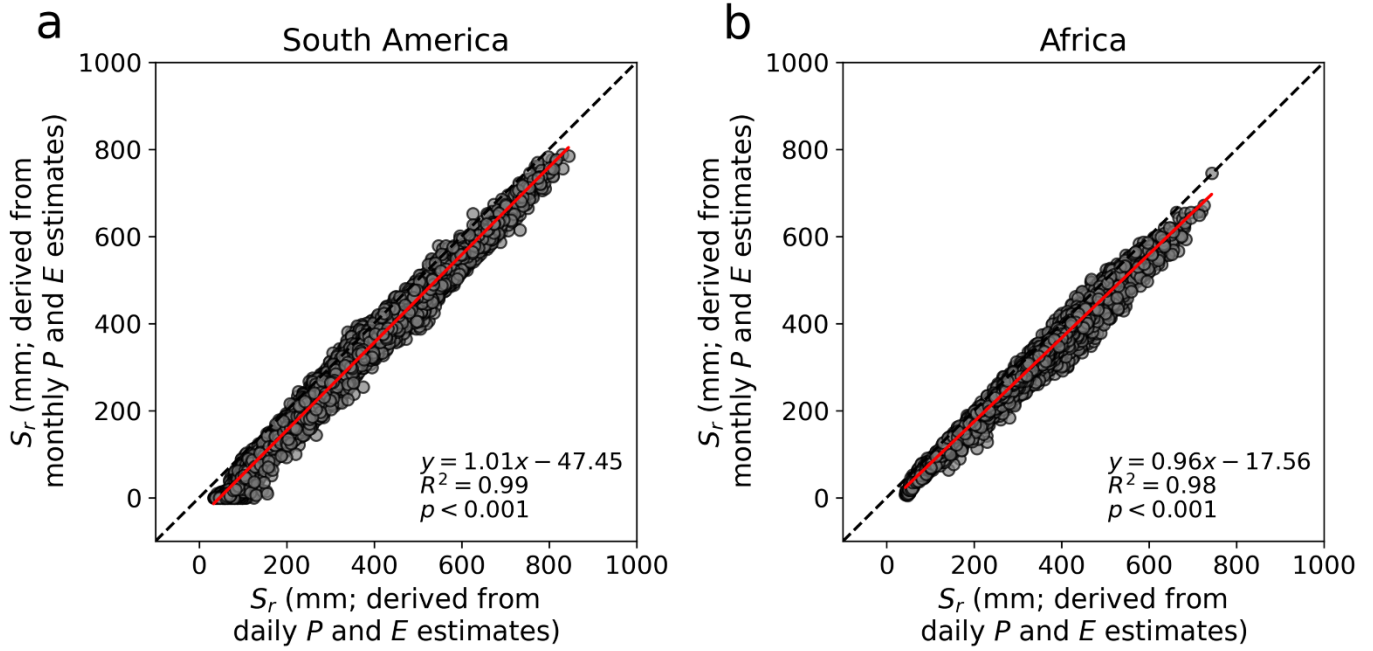


Supplementary Figure 20 | Sensitivity analysis with lower forest-savanna transition threshold. Same as Supplementary Figure 18, but for this sensitivity analysis, (a,b) we decreased the forest-savanna transition threshold for South America and Africa (relative to Figure 4).



This paper is a non-peer reviewed preprint submitted to EarthArXiv.

Supplementary Figure 21 | Sensitivity analysis with higher forest-savanna transition threshold. Same as Supplementary Figure 18, but for this sensitivity analysis, (a,b) we increased the forest-savanna transition threshold for South America and Africa (relative to Figure 4).



Supplementary Figure 22 | Comparing root zone storage capacity (S_r) based on daily and monthly estimates of precipitation (P) and evaporation (E) (both empirical; 2001-2012) for South America and Africa. Here, the regression line is represented in red, whereas the black dashed line represents the 1:1 between daily and monthly P and E derived S_r .

Supplementary Tables

Supplementary Table 1 | Overview of analysed Earth System Models (ESMs). Here, '1' represents the analysed models, whereas '0' represents models excluded from this study due to data unavailability. All ESM estimates have a variable label 'r1i1p1f1' and are downloaded at a monthly timescale. Refer to Figure 1 for more details.

Institution	ESM	Historical (2000- 2014)	SSP1-2.6 (2086- 2100)	SSP2-4.5 (2086- 2100)	SSP3-7.0 (2086- 2100)	SSP5-8.5 (2086- 2100)	For South America Lower S_r threshold = 100 mm Upper S_r threshold = 400 mm		For Africa Lower S_r threshold = 100 mm Upper S_r threshold = 350 mm	
							Percentile- eq. lower S_r threshold (mm)	Percentile- eq. upper S_r threshold (mm)	Percentile- eq. lower S_r threshold (mm)	Percentile- eq. upper S_r threshold (mm)
CSIRO-ARCCSS	ACCESS-CM2	1	1	1	1	1	116.58	409.90	121.11	310.66
CSIRO	ACCESS-ESM1-5	1	1	0	0	1	95.73	314.00	206.08	295.56
AWI	AWI-CM-1-1-MR	1	1	1	1	1	127.05	446.71	121.61	354.32
BCC	BCC-CSM2-MR	1	1	1	1	1	93.55	348.75	67.83	134.38
CAS	CAS-ESM2-0	1	1	1	1	1	120.42	336.19	49.69	220.27
NCAR	CESM2-WACCM	1	1	1	1	1	164.95	445.45	129.92	316.43
CMCC	CMCC-CM2-SR5	1	1	1	1	1	155.17	288.22	110.77	204.21
CMCC	CMCC-ESM2	1	1	1	1	1	147.60	282.74	122.63	203.50
CCCMA	CanESM5	1	1	1	1	1	194.05	337.46	258.61	422.44
E3SM-PROJECT	E3SM-1-1	1	0	0	0	1	165.40	338.41	110.79	217.85
EC-EARTH-CONSORTIUM	EC-Earth3	1	1	1	1	1	109.69	295.35	220.38	297.82
EC-EARTH-CONSORTIUM	EC-Earth3-AerChem	1	0	0	1	0	148.24	290.57	190.16	283.32
EC-EARTH-CONSORTIUM	EC-Earth3-CC	1	0	1	0	1	133.02	295.08	212.84	291.76
EC-EARTH-CONSORTIUM	EC-Earth3-Veg-LR	1	1	1	1	1	140.76	287.43	219.32	298.82
CAS	FGOALS-f3-L	1	1	1	1	1	132.62	211.54	8.59	158.33

This paper is a non-peer reviewed preprint submitted to EarthArXiv.

CAS	FGOALS-g3	1	1	1	1	1	50.59	237.41	87.84	175.73
FIO-QLNM	FIO-ESM-2-0	1	1	1	0	1	175.22	389.88	171.90	281.87
NOAA-GFDL	GFDL-CM4	1	0	1	0	1	236.71	503.84	234.74	392.20
NOAA-GFDL	GFDL-ESM4	1	1	1	1	1	218.29	448.12	264.17	378.16
CCCR-IITM	IITM-ESM*	1	0	1	1	1	61.79	178.84	53.05	143.62
INM	INM-CM4-8	1	1	1	1	1	160.64	213.78	87.85	193.70
INM	INM-CM5-0	1	1	1	1	1	176.90	211.89	81.61	208.74
IPSL	IPSL-CM5A2- INCA	1	0	0	1	0	108.53	518.70	195.46	298.38
IPSL	IPSL-CM6A-LR	1	1	1	1	1	81.03	286.70	121.64	201.10
NIMS-KMA	KACE-1-0-G	1	1	1	1	1	0.98	24.42	5.28	19.71
MIROC	MIROC6	1	1	1	1	1	162.82	512.90	194.18	405.90
MPI-M/DKRZ	MPI-ESM1-2- HR	1	1	1	1	1	107.09	402.43	125.14	379.69
MPI-M	MPI-ESM1-2- LR	1	1	1	1	1	150.71	442.32	153.40	379.91
MRI	MRI-ESM2-0	1	1	1	1	1	184.23	620.21	270.23	334.59
NUIST	NESM3	1	1	1	0	1	225.25	501.55	304.84	514.99
NCC	NorESM2-LM	1	1	1	1	0	228.73	499.49	183.81	312.88
NCC	NorESM2-MM	1	1	1	1	1	154.86	414.64	164.23	309.66
AS-RCEC	TaiESM1	1	1	1	1	1	183.25	392.83	173.93	297.18
	(Total)	33	27	29	27	30				

* IITM-ESM simulations are only available between 2015-2099, except for the SSP3-7.0 scenario, for which data is available between 2015-2098.

Supplementary Table 2 | Citations for CMIP6 datasets used in this study.

Institution	ESM	Historical	SSP1-2.6	SSP2-4.5	SSP3-7.0	SSP5-8.5
CSIRO-ARCCSS	ACCESS-CM2	Dix et al. (2019). CSIRO-ARCCSS ACCESS-CM2 model output prepared for CMIP6 CMIP historical. Earth System Grid Federation. doi:https://doi.org/10.22033/ESGF/CMIP6.4271 .	Dix et al. (2019). CSIRO-ARCCSS ACCESS-CM2 model output prepared for CMIP6 ScenarioMIP ssp126. Earth System Grid Federation. doi:https://doi.org/10.22033/ESGF/CMIP6.4319 .	Dix et al. (2019). CSIRO-ARCCSS ACCESS-CM2 model output prepared for CMIP6 ScenarioMIP ssp245. Earth System Grid Federation. doi:https://doi.org/10.22033/ESGF/CMIP6.4321 .	Dix et al. (2019). CSIRO-ARCCSS ACCESS-CM2 model output prepared for CMIP6 ScenarioMIP ssp370. Earth System Grid Federation. doi:https://doi.org/10.22033/ESGF/CMIP6.4323 .	Dix et al. (2019). CSIRO-ARCCSS ACCESS-CM2 model output prepared for CMIP6 ScenarioMIP ssp585. Earth System Grid Federation. doi:https://doi.org/10.22033/ESGF/CMIP6.4332 .
CSIRO	ACCESS-ESM1-5	Ziehn et al. (2019). CSIRO ACCESS-ESM1.5 model output prepared for CMIP6 CMIP historical. Earth System Grid Federation. doi:https://doi.org/10.22033/ESGF/CMIP6.4272 .	Ziehn et al. (2019). CSIRO ACCESS-ESM1.5 model output prepared for CMIP6 ScenarioMIP ssp126. Earth System Grid Federation. doi:https://doi.org/10.22033/ESGF/CMIP6.4320 .			Ziehn et al. (2019). CSIRO ACCESS-ESM1.5 model output prepared for CMIP6 ScenarioMIP ssp585. Earth System Grid Federation. doi:https://doi.org/10.22033/ESGF/CMIP6.4333 .
AWI	AWI-CM1-1-MR	Semmler et al. (2018). AWI AWI-CM1.1MR model output prepared for CMIP6 CMIP historical. Earth System Grid Federation. doi:https://doi.org/10.22033/ESGF/CMIP6.2686 .	Semmler et al. (2018). AWI AWI-CM1.1MR model output prepared for CMIP6 ScenarioMIP ssp126. Earth System Grid Federation. doi:https://doi.org/10.22033/ESGF/CMIP6.2796 .	Semmler et al. (2018). AWI AWI-CM1.1MR model output prepared for CMIP6 ScenarioMIP ssp245. Earth System Grid Federation. doi:https://doi.org/10.22033/ESGF/CMIP6.2800 .	Semmler et al. (2019). AWI AWI-CM1.1MR model output prepared for CMIP6 ScenarioMIP ssp370. Earth System Grid Federation. doi:https://doi.org/10.22033/ESGF/CMIP6.2803 .	Semmler et al. (2019). AWI AWI-CM1.1MR model output prepared for CMIP6 ScenarioMIP ssp585. Earth System Grid Federation. doi:https://doi.org/10.22033/ESGF/CMIP6.2817 .
BCC	BCC-CSM2-MR	Wu et al. (2018). BCC BCC-CSM2MR model output prepared for CMIP6 CMIP historical. Earth System Grid Federation. doi:https://doi.org/10.22033/ESGF/CMIP6.2948 .	Xin et al. (2019). BCC BCC-CSM2MR model output prepared for CMIP6 ScenarioMIP ssp126. Earth System Grid Federation. doi:https://doi.org/10.22033/ESGF/CMIP6.3028 .	Xin et al. (2019). BCC BCC-CSM2MR model output prepared for CMIP6 ScenarioMIP ssp245. Earth System Grid Federation. doi:https://doi.org/10.22033/ESGF/CMIP6.3030 .	Xin et al. (2019). BCC BCC-CSM2MR model output prepared for CMIP6 ScenarioMIP ssp370. Earth System Grid Federation. doi:https://doi.org/10.22033/ESGF/CMIP6.3035 .	Xin et al. (2019). BCC BCC-CSM2MR model output prepared for CMIP6 ScenarioMIP ssp585. Earth System Grid Federation. doi:https://doi.org/10.22033/ESGF/CMIP6.3050 .
CAS	CAS-ESM2-0	Chai, Zhaoyang (2020). CAS CAS-ESM1.0 model output prepared for CMIP6 CMIP historical. Earth System Grid Federation. doi:https://doi.org/10.22033/ESGF/CMIP6.3353 .	(2018). CAS CAS-ESM1.0 model output prepared for CMIP6 ScenarioMIP ssp126. Earth System Grid Federation. http://cera-www.dkrz.de/WDCC/meta/CMIP6/CMIP6.ScenarioMIP.CAS.CAS-ESM2-0.ssp126	(2018). CAS CAS-ESM1.0 model output prepared for CMIP6 ScenarioMIP ssp245. Earth System Grid Federation. http://cera-www.dkrz.de/WDCC/meta/CMIP6/CMIP6.ScenarioMIP.CAS.CAS-ESM2-0.ssp245	(2018). CAS CAS-ESM1.0 model output prepared for CMIP6 ScenarioMIP ssp370. Earth System Grid Federation. http://cera-www.dkrz.de/WDCC/meta/CMIP6/CMIP6.ScenarioMIP.CAS.CAS-ESM2-0.ssp370	(2018). CAS CAS-ESM1.0 model output prepared for CMIP6 ScenarioMIP ssp585. Earth System Grid Federation. http://cera-www.dkrz.de/WDCC/meta/CMIP6/CMIP6.ScenarioMIP.CAS.CAS-ESM2-0.ssp585
NCAR	CESM2-WACCM	Danabasoglu, Gokhan (2019). NCAR CESM2-WACCM model output prepared for CMIP6 CMIP historical. Earth System Grid Federation. doi:https://doi.org/10.22033/ESGF/CMIP6.10071 .	Danabasoglu, Gokhan (2019). NCAR CESM2-WACCM model output prepared for CMIP6 ScenarioMIP ssp126. Earth System Grid Federation. doi:https://doi.org/10.22033/ESGF/CMIP6.10100 .	Danabasoglu, Gokhan (2019). NCAR CESM2-WACCM model output prepared for CMIP6 ScenarioMIP ssp245. Earth System Grid Federation. doi:https://doi.org/10.22033/ESGF/CMIP6.10101 .	Danabasoglu, Gokhan (2019). NCAR CESM2-WACCM model output prepared for CMIP6 ScenarioMIP ssp370. Earth System Grid Federation. doi:https://doi.org/10.22033/ESGF/CMIP6.10102 .	Danabasoglu, Gokhan (2019). NCAR CESM2-WACCM model output prepared for CMIP6 ScenarioMIP ssp585. Earth System Grid Federation. doi:https://doi.org/10.22033/ESGF/CMIP6.10115 .

This paper is a non-peer reviewed preprint submitted to EarthArXiv.

CMCC	CMCC-CM2-SR5	Lovato et al. (2020). CMCC CMCC-CM2-SR5 model output prepared for CMIP6 CMIP historical. Earth System Grid Federation. doi: https://doi.org/10.22033/ESGF/CMIP6.3825 .	Lovato et al. (2020). CMCC CMCC-CM2-SR5 model output prepared for CMIP6 ScenarioMIP ssp126. Earth System Grid Federation. doi: https://doi.org/10.22033/ESGF/CMIP6.3887 .	Lovato et al. (2020). CMCC CMCC-CM2-SR5 model output prepared for CMIP6 ScenarioMIP ssp245. Earth System Grid Federation. doi: https://doi.org/10.22033/ESGF/CMIP6.3889 .	Lovato et al. (2020). CMCC CMCC-CM2-SR5 model output prepared for CMIP6 ScenarioMIP ssp370. Earth System Grid Federation. doi: https://doi.org/10.22033/ESGF/CMIP6.3890 .	Lovato et al. (2020). CMCC CMCC-CM2-SR5 model output prepared for CMIP6 ScenarioMIP ssp585. Earth System Grid Federation. doi: https://doi.org/10.22033/ESGF/CMIP6.3896 .
CMCC	CMCC-ESM2	Lovato et al. (2021). CMCC CMCC-ESM2 model output prepared for CMIP6 CMIP historical. Earth System Grid Federation. doi: https://doi.org/10.22033/ESGF/CMIP6.13195 .	Lovato et al. (2021). CMCC CMCC-ESM2 model output prepared for CMIP6 ScenarioMIP ssp126. Earth System Grid Federation. doi: https://doi.org/10.22033/ESGF/CMIP6.13250 .	Lovato et al. (2021). CMCC CMCC-ESM2 model output prepared for CMIP6 ScenarioMIP ssp245. Earth System Grid Federation. doi: https://doi.org/10.22033/ESGF/CMIP6.13252 .	Lovato et al. (2021). CMCC CMCC-ESM2 model output prepared for CMIP6 ScenarioMIP ssp370. Earth System Grid Federation. doi: https://doi.org/10.22033/ESGF/CMIP6.13253 .	Lovato et al. (2021). CMCC CMCC-ESM2 model output prepared for CMIP6 ScenarioMIP ssp585. Earth System Grid Federation. doi: https://doi.org/10.22033/ESGF/CMIP6.13259 .
CCCMA	CanESM5	Swart et al. (2019). CCCma CanESM5 model output prepared for CMIP6 CMIP historical. Earth System Grid Federation. doi: https://doi.org/10.22033/ESGF/CMIP6.3610 .	Swart et al. (2019). CCCma CanESM5 model output prepared for CMIP6 ScenarioMIP ssp126. Earth System Grid Federation. doi: https://doi.org/10.22033/ESGF/CMIP6.3683 .	Swart et al. (2019). CCCma CanESM5 model output prepared for CMIP6 ScenarioMIP ssp245. Earth System Grid Federation. doi: https://doi.org/10.22033/ESGF/CMIP6.3685 .	Swart et al. (2019). CCCma CanESM5 model output prepared for CMIP6 ScenarioMIP ssp370. Earth System Grid Federation. doi: https://doi.org/10.22033/ESGF/CMIP6.3690 .	Swart et al. (2019). CCCma CanESM5 model output prepared for CMIP6 ScenarioMIP ssp585. Earth System Grid Federation. doi: https://doi.org/10.22033/ESGF/CMIP6.3696 .
E3SM-PROJECT	E3SM-1-1	Bader et al. (2019). E3SM-Project E3SM1.1 model output prepared for CMIP6 CMIP historical. Earth System Grid Federation. doi: https://doi.org/10.22033/ESGF/CMIP6.11485 .				Bader et al. (2020). E3SM-Project E3SM1.1 model output prepared for CMIP6 ScenarioMIP ssp585. Earth System Grid Federation. doi: https://doi.org/10.22033/ESGF/CMIP6.15179 .
EC-EARTH-CONSORTIUM	EC-Earth3	EC-Earth Consortium (EC-Earth) (2019). EC-Earth-Consortium EC-Earth3 model output prepared for CMIP6 CMIP historical. Earth System Grid Federation. doi: https://doi.org/10.22033/ESGF/CMIP6.4700 .	EC-Earth Consortium (EC-Earth) (2019). EC-Earth-Consortium EC-Earth3 model output prepared for CMIP6 ScenarioMIP ssp126. Earth System Grid Federation. doi: https://doi.org/10.22033/ESGF/CMIP6.4874 .	EC-Earth Consortium (EC-Earth) (2019). EC-Earth-Consortium EC-Earth3 model output prepared for CMIP6 ScenarioMIP ssp245. Earth System Grid Federation. doi: https://doi.org/10.22033/ESGF/CMIP6.4880 .	EC-Earth Consortium (EC-Earth) (2019). EC-Earth-Consortium EC-Earth3 model output prepared for CMIP6 ScenarioMIP ssp370. Earth System Grid Federation. doi: https://doi.org/10.22033/ESGF/CMIP6.4884 .	EC-Earth Consortium (EC-Earth) (2019). EC-Earth-Consortium EC-Earth3 model output prepared for CMIP6 ScenarioMIP ssp585. Earth System Grid Federation. doi: https://doi.org/10.22033/ESGF/CMIP6.4912 .
EC-EARTH-CONSORTIUM	EC-Earth3-AerChem	EC-Earth Consortium (EC-Earth) (2020). EC-Earth-Consortium EC-Earth3-AerChem model output prepared for CMIP6 CMIP historical. Earth System Grid Federation. doi: https://doi.org/10.22033/ESGF/CMIP6.4701 .			EC-Earth Consortium (EC-Earth) (2020). EC-Earth-Consortium EC-Earth3-AerChem model output prepared for CMIP6 ScenarioMIP ssp370. Earth System Grid Federation. doi: https://doi.org/10.22033/ESGF/CMIP6.4885 .	

This paper is a non-peer reviewed preprint submitted to EarthArXiv.

EC-EARTH-CONSORTIUM	EC-Earth3-CC	EC-Earth Consortium (EC-Earth) (2021). EC-Earth-Consortium EC-Earth3-CC model output prepared for CMIP6 CMIP historical. Earth System Grid Federation. doi:https://doi.org/10.22033/ESGF/CMIP6.4702 .		EC-Earth Consortium (EC-Earth) (2021). EC-Earth-Consortium EC-Earth3-CC model output prepared for CMIP6 ScenarioMIP ssp245. Earth System Grid Federation. doi:https://doi.org/10.22033/ESGF/CMIP6.15631 .		EC-Earth Consortium (EC-Earth) (2021). EC-Earth-Consortium EC-Earth3-CC model output prepared for CMIP6 ScenarioMIP ssp585. Earth System Grid Federation. doi:https://doi.org/10.22033/ESGF/CMIP6.15636 .
EC-EARTH-CONSORTIUM	EC-Earth3-Veg-LR	EC-Earth Consortium (EC-Earth) (2020). EC-Earth-Consortium EC-Earth3-Veg-LR model output prepared for CMIP6 CMIP historical. Earth System Grid Federation. doi:https://doi.org/10.22033/ESGF/CMIP6.4707 .	EC-Earth Consortium (EC-Earth) (2020). EC-Earth-Consortium EC-Earth3-Veg-LR model output prepared for CMIP6 ScenarioMIP ssp126. Earth System Grid Federation. doi:https://doi.org/10.22033/ESGF/CMIP6.4877 .	EC-Earth Consortium (EC-Earth) (2020). EC-Earth-Consortium EC-Earth3-Veg-LR model output prepared for CMIP6 ScenarioMIP ssp245. Earth System Grid Federation. doi:https://doi.org/10.22033/ESGF/CMIP6.4883 .	EC-Earth Consortium (EC-Earth) (2020). EC-Earth-Consortium EC-Earth3-Veg-LR model output prepared for CMIP6 ScenarioMIP ssp370. Earth System Grid Federation. doi:https://doi.org/10.22033/ESGF/CMIP6.4887 .	EC-Earth Consortium (EC-Earth) (2020). EC-Earth-Consortium EC-Earth3-Veg-LR model output prepared for CMIP6 ScenarioMIP ssp585. Earth System Grid Federation. doi:https://doi.org/10.22033/ESGF/CMIP6.4915 .
CAS	FGOALS-f3-L	YU, Yongqiang (2019). CAS FGOALS-f3-L model output prepared for CMIP6 CMIP historical. Earth System Grid Federation. doi:https://doi.org/10.22033/ESGF/CMIP6.3355 .	YU, Yongqiang (2019). CAS FGOALS-f3-L model output prepared for CMIP6 ScenarioMIP ssp126. Earth System Grid Federation. doi:https://doi.org/10.22033/ESGF/CMIP6.3464 .	YU, Yongqiang (2019). CAS FGOALS-f3-L model output prepared for CMIP6 ScenarioMIP ssp245. Earth System Grid Federation. doi:https://doi.org/10.22033/ESGF/CMIP6.3468 .	YU, Yongqiang (2019). CAS FGOALS-f3-L model output prepared for CMIP6 ScenarioMIP ssp370. Earth System Grid Federation. doi:https://doi.org/10.22033/ESGF/CMIP6.3479 .	YU, Yongqiang (2019). CAS FGOALS-f3-L model output prepared for CMIP6 ScenarioMIP ssp585. Earth System Grid Federation. doi:https://doi.org/10.22033/ESGF/CMIP6.3502 .
CAS	FGOALS-g3	Li, Lijuan (2019). CAS FGOALS-g3 model output prepared for CMIP6 CMIP historical. Earth System Grid Federation. doi:https://doi.org/10.22033/ESGF/CMIP6.3356 .	Li, Lijuan (2019). CAS FGOALS-g3 model output prepared for CMIP6 ScenarioMIP ssp126. Earth System Grid Federation. doi:https://doi.org/10.22033/ESGF/CMIP6.3465 .	Li, Lijuan (2019). CAS FGOALS-g3 model output prepared for CMIP6 ScenarioMIP ssp245. Earth System Grid Federation. doi:https://doi.org/10.22033/ESGF/CMIP6.3469 .	Li, Lijuan (2019). CAS FGOALS-g3 model output prepared for CMIP6 ScenarioMIP ssp370. Earth System Grid Federation. doi:https://doi.org/10.22033/ESGF/CMIP6.3480 .	Li, Lijuan (2019). CAS FGOALS-g3 model output prepared for CMIP6 ScenarioMIP ssp585. Earth System Grid Federation. doi:https://doi.org/10.22033/ESGF/CMIP6.3503 .
FIO-QLNM	FIO-ESM2-0	Song, Zhenya; Qiao, Fangli; Bao, Ying; Shu, Qi; Song, Yajuan; Yang, Xiaodan (2019). FIO-QLNM FIO-ESM2.0 model output prepared for CMIP6 CMIP historical. Earth System Grid Federation. doi:https://doi.org/10.22033/ESGF/CMIP6.9199 .	Song, Zhenya; Qiao, Fangli; Bao, Ying; Shu, Qi; Song, Yajuan; Yang, Xiaodan (2019). FIO-QLNM FIO-ESM2.0 model output prepared for CMIP6 ScenarioMIP ssp126. Earth System Grid Federation. doi:https://doi.org/10.22033/ESGF/CMIP6.9208 .	Song, Zhenya; Qiao, Fangli; Bao, Ying; Shu, Qi; Song, Yajuan; Yang, Xiaodan (2019). FIO-QLNM FIO-ESM2.0 model output prepared for CMIP6 ScenarioMIP ssp245. Earth System Grid Federation. doi:https://doi.org/10.22033/ESGF/CMIP6.9209 .		Song, Zhenya; Qiao, Fangli; Bao, Ying; Shu, Qi; Song, Yajuan; Yang, Xiaodan (2019). FIO-QLNM FIO-ESM2.0 model output prepared for CMIP6 ScenarioMIP ssp585. Earth System Grid Federation. doi:https://doi.org/10.22033/ESGF/CMIP6.9214 .
NOAA-GFDL	GFDL-CM4	Guo et al. (2018). NOAA-GFDL GFDL-CM4 model output historical. Earth System Grid Federation. doi:https://doi.org/10.22033/ESGF/CMIP6.8594 .		Guo et al. (2018). NOAA-GFDL GFDL-CM4 model output prepared for CMIP6 ScenarioMIP ssp245. Earth System Grid Federation. doi:https://doi.org/10.22033/ESGF/CMIP6.9263 .		Guo et al. (2018). NOAA-GFDL GFDL-CM4 model output prepared for CMIP6 ScenarioMIP ssp585. Earth System Grid Federation. doi:https://doi.org/10.22033/ESGF/CMIP6.9268 .

This paper is a non-peer reviewed preprint submitted to EarthArXiv.

NOAA-GFDL	GFDL-ESM4	Krasting et al. (2018). NOAA-GFDL GFDL-ESM4 model output prepared for CMIP6 CMIP historical. Earth System Grid Federation. doi:https://doi.org/10.22033/ESGF/CMIP6.8597 .	John et al. (2018). NOAA-GFDL GFDL-ESM4 model output prepared for CMIP6 ScenarioMIP ssp126. Earth System Grid Federation. doi:https://doi.org/10.22033/ESGF/CMIP6.8684 .	John et al. (2018). NOAA-GFDL GFDL-ESM4 model output prepared for CMIP6 ScenarioMIP ssp245. Earth System Grid Federation. doi:https://doi.org/10.22033/ESGF/CMIP6.8686 .	John et al. (2018). NOAA-GFDL GFDL-ESM4 model output prepared for CMIP6 ScenarioMIP ssp370. Earth System Grid Federation. doi:https://doi.org/10.22033/ESGF/CMIP6.8691 .	John et al. (2018). NOAA-GFDL GFDL-ESM4 model output prepared for CMIP6 ScenarioMIP ssp585. Earth System Grid Federation. doi:https://doi.org/10.22033/ESGF/CMIP6.8706 .
CCCR-IITM	IITM-ESM	Choudhury et al. (2019). CCCR-IITM IITM-ESM model output prepared for CMIP6 CMIP historical. Earth System Grid Federation. doi:https://doi.org/10.22033/ESGF/CMIP6.3708 .		Singh et al. (2020). CCCR-IITM IITM-ESM model output prepared for CMIP6 ScenarioMIP ssp245. Earth System Grid Federation. doi:https://doi.org/10.22033/ESGF/CMIP6.14748 .	Gopinathan et al. (2020). CCCR-IITM IITM-ESM model output prepared for CMIP6 ScenarioMIP ssp370. Earth System Grid Federation. doi:https://doi.org/10.22033/ESGF/CMIP6.14749 .	Panickal et al. (2020). CCCR-IITM IITM-ESM model output prepared for CMIP6 ScenarioMIP ssp585. Earth System Grid Federation. doi:https://doi.org/10.22033/ESGF/CMIP6.14753 .
INM	INM-CM4-8	Volodin et al. (2019). INM INM-CM4-8 model output prepared for CMIP6 CMIP historical. Earth System Grid Federation. doi:https://doi.org/10.22033/ESGF/CMIP6.5069 .	Volodin et al. (2019). INM INM-CM4-8 model output prepared for CMIP6 ScenarioMIP ssp126. Earth System Grid Federation. doi:https://doi.org/10.22033/ESGF/CMIP6.12325 .	Volodin et al. (2019). INM INM-CM4-8 model output prepared for CMIP6 ScenarioMIP ssp245. Earth System Grid Federation. doi:https://doi.org/10.22033/ESGF/CMIP6.12327 .	Volodin et al. (2019). INM INM-CM4-8 model output prepared for CMIP6 ScenarioMIP ssp370. Earth System Grid Federation. doi:https://doi.org/10.22033/ESGF/CMIP6.12329 .	Volodin et al. (2019). INM INM-CM4-8 model output prepared for CMIP6 ScenarioMIP ssp585. Earth System Grid Federation. doi:https://doi.org/10.22033/ESGF/CMIP6.12337 .
INM	INM-CM5-0	Volodin et al. (2019). INM INM-CM5-0 model output prepared for CMIP6 CMIP historical. Earth System Grid Federation. doi:https://doi.org/10.22033/ESGF/CMIP6.5070 .	Volodin et al. (2019). INM INM-CM5-0 model output prepared for CMIP6 ScenarioMIP ssp126. Earth System Grid Federation. doi:https://doi.org/10.22033/ESGF/CMIP6.12326 .	Volodin et al. (2019). INM INM-CM5-0 model output prepared for CMIP6 ScenarioMIP ssp245. Earth System Grid Federation. doi:https://doi.org/10.22033/ESGF/CMIP6.12328 .	Volodin et al. (2019). INM INM-CM5-0 model output prepared for CMIP6 ScenarioMIP ssp370. Earth System Grid Federation. doi:https://doi.org/10.22033/ESGF/CMIP6.12330 .	Volodin et al. (2019). INM INM-CM5-0 model output prepared for CMIP6 ScenarioMIP ssp585. Earth System Grid Federation. doi:https://doi.org/10.22033/ESGF/CMIP6.12338 .
IPSL	IPSL-CM5A2-INCA	Bouche et al. (2020). IPSL IPSL-CM5A2-INCA model output prepared for CMIP6 CMIP historical. Earth System Grid Federation. doi:https://doi.org/10.22033/ESGF/CMIP6.13661 .			Boucher et al. (2020). IPSL IPSL-CM5A2-INCA model output prepared for CMIP6 ScenarioMIP ssp370. Earth System Grid Federation. doi:https://doi.org/10.22033/ESGF/CMIP6.15714 .	
IPSL	IPSL-CM6A-LR	Boucher et al. (2018). IPSL IPSL-CM6A-LR model output prepared for CMIP6 CMIP historical. Earth System Grid Federation. doi:https://doi.org/10.22033/ESGF/CMIP6.5195 .	Boucher et al. (2019). IPSL IPSL-CM6A-LR model output prepared for CMIP6 ScenarioMIP ssp126. Earth System Grid Federation. doi:https://doi.org/10.22033/ESGF/CMIP6.5262 .	Boucher et al. (2019). IPSL IPSL-CM6A-LR model output prepared for CMIP6 ScenarioMIP ssp245. Earth System Grid Federation. doi:https://doi.org/10.22033/ESGF/CMIP6.5264 .	Boucher et al. (2019). IPSL IPSL-CM6A-LR model output prepared for CMIP6 ScenarioMIP ssp370. Earth System Grid Federation. doi:https://doi.org/10.22033/ESGF/CMIP6.5265 .	Bouche et al. (2019). IPSL IPSL-CM6A-LR model output prepared for CMIP6 ScenarioMIP ssp585. Earth System Grid Federation. doi:https://doi.org/10.22033/ESGF/CMIP6.5271 .

This paper is a non-peer reviewed preprint submitted to EarthArXiv.

NIMS-KMA	KACE-1.0-G	Byun et al. (2019). NIMS-KMA KACE1.0-G model output prepared for CMIP6 CMIP historical. Earth System Grid Federation. doi: https://doi.org/10.22033/ESGF/CMIP6.8378 .	Byun et al. (2019). NIMS-KMA KACE1.0-G model output prepared for CMIP6 ScenarioMIP ssp126. Earth System Grid Federation. doi: https://doi.org/10.22033/ESGF/CMIP6.8432 .	Byun et al. (2019). NIMS-KMA KACE1.0-G model output prepared for CMIP6 ScenarioMIP ssp245. Earth System Grid Federation. doi: https://doi.org/10.22033/ESGF/CMIP6.8435 .	Byun et al. (2019). NIMS-KMA KACE1.0-G model output prepared for CMIP6 ScenarioMIP ssp370. Earth System Grid Federation. doi: https://doi.org/10.22033/ESGF/CMIP6.8437 .	Byun et al. (2019). NIMS-KMA KACE1.0-G model output prepared for CMIP6 ScenarioMIP ssp585. Earth System Grid Federation. doi: https://doi.org/10.22033/ESGF/CMIP6.8456 .
MIROC	MIROC6	Tatebe et al. (2018). MIROC MIROC6 model output prepared for CMIP6 CMIP historical. Earth System Grid Federation. doi: https://doi.org/10.22033/ESGF/CMIP6.5603 .	Shiogama et al. (2019). MIROC MIROC6 model output prepared for CMIP6 ScenarioMIP ssp126. Earth System Grid Federation. doi: https://doi.org/10.22033/ESGF/CMIP6.5743 .	Shiogama et al. (2019). MIROC MIROC6 model output prepared for CMIP6 ScenarioMIP ssp245. Earth System Grid Federation. doi: https://doi.org/10.22033/ESGF/CMIP6.5746 .	Shiogama et al. (2019). MIROC MIROC6 model output prepared for CMIP6 ScenarioMIP ssp370. Earth System Grid Federation. doi: https://doi.org/10.22033/ESGF/CMIP6.5752 .	Shiogama et al. (2019). MIROC MIROC6 model output prepared for CMIP6 ScenarioMIP ssp585. Earth System Grid Federation. doi: https://doi.org/10.22033/ESGF/CMIP6.5771 .
MPI-M/DKRZ	MPI-ESM1-2-HR	Jungclaus et al. (2019). MPI-M MPI-ESM1.2-HR model output prepared for CMIP6 CMIP historical. Earth System Grid Federation. doi: https://doi.org/10.22033/ESGF/CMIP6.6594 .	Schupfner et al. (2019). DKRZ MPI-ESM1.2-HR model output prepared for CMIP6 ScenarioMIP ssp126. Earth System Grid Federation. doi: https://doi.org/10.22033/ESGF/CMIP6.4397 .	Schupfner et al. (2019). DKRZ MPI-ESM1.2-HR model output prepared for CMIP6 ScenarioMIP ssp245. Earth System Grid Federation. doi: https://doi.org/10.22033/ESGF/CMIP6.4398 .	Schupfner et al. (2019). DKRZ MPI-ESM1.2-HR model output prepared for CMIP6 ScenarioMIP ssp370. Earth System Grid Federation. doi: https://doi.org/10.22033/ESGF/CMIP6.4399 .	Schupfner et al. (2019). DKRZ MPI-ESM1.2-HR model output prepared for CMIP6 ScenarioMIP ssp585. Earth System Grid Federation. doi: https://doi.org/10.22033/ESGF/CMIP6.4403 .
MPI-M	MPI-ESM1-2-LR	Wieners et al. (2019). MPI-M MPI-ESM1.2-LR model output prepared for CMIP6 CMIP historical. Earth System Grid Federation. doi: https://doi.org/10.22033/ESGF/CMIP6.6595 .	Wieners et al. (2019). MPI-M MPI-ESM1.2-LR model output prepared for CMIP6 ScenarioMIP ssp126. Earth System Grid Federation. doi: https://doi.org/10.22033/ESGF/CMIP6.6690 .	Wieners et al. (2019). MPI-M MPI-ESM1.2-LR model output prepared for CMIP6 ScenarioMIP ssp245. Earth System Grid Federation. doi: https://doi.org/10.22033/ESGF/CMIP6.6693 .	Wieners et al. (2019). MPI-M MPI-ESM1.2-LR model output prepared for CMIP6 ScenarioMIP ssp370. Earth System Grid Federation. doi: https://doi.org/10.22033/ESGF/CMIP6.6695 .	Wieners et al. (2019). MPI-M MPI-ESM1.2-LR model output prepared for CMIP6 ScenarioMIP ssp585. Earth System Grid Federation. doi: https://doi.org/10.22033/ESGF/CMIP6.6705 .
MRI	MRI-ESM2-0	Yukimoto et al. (2019). MRI MRI-ESM2.0 model output prepared for CMIP6 CMIP historical. Earth System Grid Federation. doi: https://doi.org/10.22033/ESGF/CMIP6.6842 .	Yukimoto et al. (2019). MRI MRI-ESM2.0 model output prepared for CMIP6 ScenarioMIP ssp126. Earth System Grid Federation. doi: https://doi.org/10.22033/ESGF/CMIP6.6909 .	Yukimoto et al. (2019). MRI MRI-ESM2.0 model output prepared for CMIP6 ScenarioMIP ssp245. Earth System Grid Federation. doi: https://doi.org/10.22033/ESGF/CMIP6.6910 .	Yukimoto et al. (2019). MRI MRI-ESM2.0 model output prepared for CMIP6 ScenarioMIP ssp370. Earth System Grid Federation. doi: https://doi.org/10.22033/ESGF/CMIP6.6915 .	Yukimoto et al. (2019). MRI MRI-ESM2.0 model output prepared for CMIP6 ScenarioMIP ssp585. Earth System Grid Federation. doi: https://doi.org/10.22033/ESGF/CMIP6.6929 .
NUIST	NESM3	Cao, Jian; Wang, Bin (2019). NUIST NESMv3 model output prepared for CMIP6 CMIP historical. Earth System Grid Federation. doi: https://doi.org/10.22033/ESGF/CMIP6.8769 .	Cao, Jian (2019). NUIST NESMv3 model output prepared for CMIP6 ScenarioMIP ssp126. Earth System Grid Federation. doi: https://doi.org/10.22033/ESGF/CMIP6.8780 .	Cao, Jian (2019). NUIST NESMv3 model output prepared for CMIP6 ScenarioMIP ssp245. Earth System Grid Federation. doi: https://doi.org/10.22033/ESGF/CMIP6.8781 .		Cao, Jian (2019). NUIST NESMv3 model output prepared for CMIP6 ScenarioMIP ssp585. Earth System Grid Federation. doi: https://doi.org/10.22033/ESGF/CMIP6.8790 .
NCC	NorESM2-LM	Seland et al. (2019). NCC NorESM2-LM model output prepared for CMIP6 CMIP historical. Earth System Grid Federation. doi: https://doi.org/10.22033/ESGF/CMIP6.8036 .	Seland et al. (2019). NCC NorESM2-LM model output prepared for CMIP6 ScenarioMIP ssp126. Earth System Grid Federation. doi: https://doi.org/10.22033/ESGF/CMIP6.8248 .	Seland et al. (2019). NCC NorESM2-LM model output prepared for CMIP6 ScenarioMIP ssp245. Earth System Grid Federation. doi: https://doi.org/10.22033/ESGF/CMIP6.8253 .	Seland et al. (2019). NCC NorESM2-LM model output prepared for CMIP6 ScenarioMIP ssp370. Earth System Grid Federation. doi: https://doi.org/10.22033/ESGF/CMIP6.8268 .	

This paper is a non-peer reviewed preprint submitted to EarthArXiv.

NCC	NorESM2-MM	Bentsen et al. (2019). NCC NorESM2-MM model output prepared for CMIP6 CMIP historical. Earth System Grid Federation. doi: https://doi.org/10.22033/ESGF/CMIP6.8040 .	Bentsen et al. (2019). NCC NorESM2-MM model output prepared for CMIP6 ScenarioMIP ssp126. Earth System Grid Federation. doi: https://doi.org/10.22033/ESGF/CMIP6.8250 .	Bentsen et al. (2019). NCC NorESM2-MM model output prepared for CMIP6 ScenarioMIP ssp245. Earth System Grid Federation. doi: https://doi.org/10.22033/ESGF/CMIP6.8255 .	Bentsen et al. (2019). NCC NorESM2-MM model output prepared for CMIP6 ScenarioMIP ssp370. Earth System Grid Federation. doi: https://doi.org/10.22033/ESGF/CMIP6.8270 .	Bentsen et al. (2019). NCC NorESM2-MM model output prepared for CMIP6 ScenarioMIP ssp585. Earth System Grid Federation. doi: https://doi.org/10.22033/ESGF/CMIP6.8321 .
AS-RCEC	TaiESM1	Lee, Wei-Liang; Liang, Hsin-Chien (2020). AS-RCEC TaiESM1.0 model output prepared for CMIP6 CMIP historical. Earth System Grid Federation. doi: https://doi.org/10.22033/ESGF/CMIP6.9755 .	Lee, Wei-Liang; Liang, Hsin-Chien (2020). AS-RCEC TaiESM1.0 model output prepared for CMIP6 ScenarioMIP ssp126. Earth System Grid Federation. doi: https://doi.org/10.22033/ESGF/CMIP6.9806 .	Lee, Wei-Liang; Liang, Hsin-Chien (2020). AS-RCEC TaiESM1.0 model output prepared for CMIP6 ScenarioMIP ssp245. Earth System Grid Federation. doi: https://doi.org/10.22033/ESGF/CMIP6.9808 .	Lee, Wei-Liang; Liang, Hsin-Chien (2020). AS-RCEC TaiESM1.0 model output prepared for CMIP6 ScenarioMIP ssp370. Earth System Grid Federation. doi: https://doi.org/10.22033/ESGF/CMIP6.9809 .	Lee, Wei-Liang; Liang, Hsin-Chien (2020). AS-RCEC TaiESM1.0 model output prepared for CMIP6 ScenarioMIP ssp585. Earth System Grid Federation. doi: https://doi.org/10.22033/ESGF/CMIP6.9823 .

Supplementary References

1. Singh, C., Wang-Erlandsson, L., Fetzer, I., Rockström, J. & Ent, R. van der. Rootzone storage capacity reveals drought coping strategies along rainforest-savanna transitions. *Environ. Res. Lett.* **15**, 124021 (2020).
2. Wang-Erlandsson, L. *et al.* Global root zone storage capacity from satellite-based evaporation. *Hydrology and Earth System Sciences* **20**, 1459–1481 (2016).
3. de Boer-Euser, T., McMillan, H. K., Hrachowitz, M., Winsemius, H. C. & Savenije, H. H. G. Influence of soil and climate on root zone storage capacity. *Water Resources Research* **52**, 2009–2024 (2016).
4. Gao, H. *et al.* Climate controls how ecosystems size the root zone storage capacity at catchment scale: Root zone storage capacity in catchments. *Geophysical Research Letters* **41**, 7916–7923 (2014).
5. Gumbel, E. J. *Statistics of extremes*. (Columbia University Press, 1958).
6. Correoso, K. skextremes Documentation. <https://github.com/kikocorreoso/scikit-extremes> (2019).
7. ESA. GlobCover land-use map. http://due.esrin.esa.int/page_globcover.php (2010).
8. Walsh, R. P. D. & Lawler, D. M. Rainfall Seasonality: Description, Spatial Patterns and Change Through Time. *Weather* **36**, 201–208 (1981).
9. Hurtt, G. C. *et al.* Harmonization of global land use change and management for the period 850–2100 (LUH2) for CMIP6. *Geoscientific Model Development* **13**, 5425–5464 (2020).